FLOW BEHAVOIR OF GAS-CONDENSATE WELLS

A REPORT SUBMITTED TO THE DEPARTMENT OF PETROLEUM ENGINEERING

OF STANFORD UNIVERSITY

IN PARTIAL FULFILLMENT OF THE REQUIREMENTS FOR THE DEGREE OF MASTER OF SCIENCE

By

Chunmei Shi

June 2005

I certify that I have read this report and that in my opinion it is fully adequate, in scope and in quality, as partial fulfillment of the degree of Master of Science in Petroleum Engineering.

Prof. Roland N. Horne
(Principal Advisor)

Abstract

Gas-condensate reservoirs exhibit complex phase and flow behaviors due to the appearance of condensate banking in the near well region. A good understanding of the effect of the changing composition on the flow and phase behavior properties of these reservoirs is essential for carrying out accurate forecasts of the performance of gas-condensate reservoirs using numerical simulators.

This report presents an experimental phase and flow behavior analysis for a synthetic two-component gas-condensate system. The object of this work is to confirm the composition change during condensate dropout, hence to investigate the effect of composition change on gas-condensate fluid properties, such as gas relative permeability and condensate saturation.

Acknowledgments

I would like to give my sincere thanks to my advisor, Professor Roland N. Horne, for his support and guidance throughout this work. Professor Roland N. Horne has always been available to answer my questions. Without his great patience and encouragement; this work would not have been possible.

My thanks also go to Dr. Kewen Li, Chih-Ying Chen and Dr. Guoqing Tang, with whom I had a lot of discussions about the configuration of my experiment. Their insightful suggestions and help in the laboratory make this work possible.

Financial and moral support form Saudi Aramco and the members of the SUPRI-D Research Consortium on Innovation in Well Testing is greatly appreciated.

Finally, I want like to acknowledge my dear friends and colleagues for their support since I came to Stanford. Their help means so much.

Contents

Abstract v

Acknowledgments vii

Contents ix

List of Tables xi

List of Figures xiii

1. Introduction 1
2. Gas-Condensate Flow Behavoir 5
   2.1. Gas-Condensate Characterization 5
   2.2. Gas-Condensate Flow Behavior 6
      2.2.1. Phase and equilibrium behavior 6
      2.2.2. Condensate build up behavior 7
      2.2.3. Hydrocarbon composition change 9
      2.2.4. Relative permeability change 10
3. Experimental design 11
   3.1. Laboratory scale simulation 12
      3.1.1. Draw-down test simulation 12
      3.1.2. Constant pressure-drop test simulation 16
   3.2. Experimental design 19
      3.2.1. Difference between static values and flowing values 19
      3.2.2. Experimental design 19
4. Experimental Procedure 21
   4.1. Experimental Apparatus Description 21
   4.2. Gas System 23
   4.3. Experimental Procedure 25
      4.3.1. Pressure transducer calibration 25
      4.3.2. Gas Sampling 30
5. Results and Discussion 32
   5.1. Composition Changes 32
   5.2. Nitrogen Permeability Changes 35
6. Results and Discussion 32
   6.1. Conclusions 37
   6.2. Future Work 37

Nomenclature 39

References 40

A. List of Experiment Apparatus 41
B. Eclipse input data file (constant pressure drop test) 42
C. Compressibility factor for methane 47

List of Tables

Table 2.1: Composition and properties of several reservoir fluids (from CNPC report, 2001). 5
Table 5.1: Component composition results from GC analysis 33

List of Figures

Figure 2.1: Ternary visualization of hydrocarbon classification (from SPE monograph, v.20). 6
Figure 2.2: Phase diagram of a two-component methane-propane condensate system..... 7
Figure 2.3: Liquid dropout for a two-component gas-condensate system at 15 ^{o}C. 7
Figure 2.4: Schematic gas-condensate flow behavior. 8
Figure 2.5: Saturation, flowing C_{7+} fraction and pressure versus radius (from Mott, et al. 1999). 9
Figure 2.6: Shift of phase envelope with composition change (from Roussennac, 2001). 10
Figure 2.7: Input relative permeability curves for numerical simulation. 10
Figure 3.1: Phase diagram for the methane-butane system. 11
Figure 3.2: Pressure profile for draw-down test simulation. 13
Figure 3.3: Saturation profile for draw-down test simulation. 13
Figure 3.4: Overall C_4 composition change for draw-down test simulation. 14
Figure 3.5: C_4 composition profile in vapor phase for draw-down test simulation..... 14
Figure 3.6: Density profile for draw-down test simulation. 15
Figure 3.7: Draw-down test relative permeability curves..... 15
Figure 3.8: Saturation profile at different bottomhole pressure (BHP). 15
Figure 3.9: Composition profile at different bottomhole pressure (BHP)..... 16
Figure 3.10: Overall C_4 composition vs. S_c. 16
Figure 3.11: Pressure profile for constant pressure drop test simulation. 17
Figure 3.12: Condensate saturation profile for constant pressure drop test simulation.... 17
Figure 3.13: Overall C4 composition profile for constant pressure drop test simulation. 17
Figure 3.14: C_4 in vapor phase profile. 18
Figure 3.15: : Density profile for constant pressure drop simulation. 18
Figure 3.16: Constant pressure drop test relative permeability curves..... 18
Figure 3.17: Schematic diagram for static and flowing values..... 19

Figure 4.1: Pressure drop along the core-holder. 22
Figure 4.2: Schematic diagram of the gas condensate flow system. 23
Figure 4.3: Schematic diagram for Butane (C_4) transfer process. 24
Figure 4.4: Schematic diagram for Methane (C_1) transfer process..... 25
Figure 4.5: Pressure transducer 1 calibration. 26
Figure 4.6: Pressure transducer 2, 3 and 4 calibration..... 26
Figure 4.7: Pressure transducer 5 calibration. 27
Figure 4.8: Pressure transducer 6 calibration. 27
Figure 4.9: Pressure transducer 7 calibration. 27
Figure 4.10: Pressure transducer 8 calibration. 28
Figure 4.11: Pressure transducer 9 calibration. 28
Figure 4.12: Zero shift tests for pressure transducer 2. 28
Figure 4.13: Zero shift tests for pressure transducer 3. 29
Figure 4.14: Zero shift test for pressure transducer 4. 29
Figure 4.15: Measuring error under different pressure difference..... 29
Figure 4.16: Schematic diagram for gas sampling part. 31
Figure 5.1: Component compositions for different experimental tests. 34
Figure 5.2: Nitrogen permeability measurements..... 35

Chapter 1

1. Introduction

Gas-condensate reservoirs provide some of the most difficult problems in practical reservoir engineering. These reservoirs exhibit complex phase and flow behaviors due to the appearance of condensate liquid when the bottom-hole pressure drops below the dew-point pressure. The accumulated condensate in the vicinity of the well bore causes a blockage effect and reduces the effective permeability appreciably, depending on a number of reservoir and well parameters, and also causes the loss of heavy components at surface.

The productivity loss caused by the condensate buildup is striking, in some cases, the decline can be as high as a factor of two to four, according the case studies of Afidick et al. (1994) and Barnum et al. (1995). Even in very lean gas-condensate reservoirs with a maximum liquid drop out of only 1%, the productivity may be reduced by a factor of about two as the pressure drops below the dew-point pressure (Afidick et al., 1994). In order to predict well deliverability and calculate gas and liquid recovery, it is necessary to have a detailed knowledge of the relative permeability and liquid banking of gas-condensate fields.

Gas-condensate relative permeabilities depend on a number of factors associated with the fluid properties and flow process, and are affected by both viscous and capillary forces. Although research on gas-condensate systems dates back to the thirties, there are as yet no standard procedures to measure gas-condensate relative permeability. Most published studies about relative permeability, especially experimental measurements, focus on investigating the relationship between relative permeability and interfacial tension (IFT), condensate saturation, capillary number and bond number, and also the flow process, such as flow rate control.

Haniff et al. (1990) conducted an experiment using a two-component methane-propane gas-condensate system to investigate relative permeability and the interfacial tensions (IFT) relationships. They indicated that below a critical value of IFT ($0.05 mNm^{-1}$) there was a significant reduction in residual saturation and much improved flow. In this experiment, one of their experimental assumptions was that at steady-state conditions, the pressure drop across the core was constant and the upstream and downstream gas and liquid compositions would be the same. This is true for deep reservoirs where the reservoir pressure is higher than the dew-point pressure, and no liquid drops out. In the near-well region, the system pressure is usually below the dew-point pressure, so heavier components will drop out and accumulate till they reach the critical condensate saturation. In this case, composition changes are to be expected.

Later, conventional coreflood experiments on two North Sea gas-condensate reservoirs by Chen et al. (1999) explored the relative permeability decline due to the condensate drop-out and implied that critical condensate saturation (CCS) and relative permeability were sensitive to flow rate. According to their experimental observation, gas productivity impaired by condensate drop out can be somewhat restored by increasing production rate. In this experiment, it was realized that a certain amount of condensate would accumulate in the core before reaching steady-state conditions, so the condensate saturation at the end of each two-phase relative permeability measurement was estimated from the difference between injected and produced condensate volumes. Because in their study the injection gas composition changed a little, compared with what was collected in the production PVT cell, they assumed that state-steady conditions has been reached when the producing fractional flow was close to the volume fraction that had been measured in the injection cell prior to pressuring the injection fluid to single-phase conditions. This approach is reasonable since this condensate system experienced small composition change when the pressure dropped below the dew-point pressure.

Instead of measuring condensate permeability under state-steady conditions, Mott et al. (1999) applied the pseudosteady-state technique in their experiment. Suggested by Fevang and Whitson (1996), the pseudosteady-state condition was mimicked by setting

the core pressure below the dew-point pressure, while the inlet accumulator, which contains the gas-condensate fluid, had a pressure higher than the dew-point pressure. This is to simulate fluid flowing from a deep reservoir to the near-well region, where rich gas flows into a region of lower pressure, condensing liquid and increasing the liquid saturation until it is mobile. At this stage, the composition of the reservoir fluid changes from the inlet conditions to the core conditions. For this experiment, Mott et al. assumed that sometime after the pseudosteady-state stage, steady-state conditions are reached when the flowing fluid composition at the outlet of the core is the same as the gas composition in the inlet accumulator. Then the relative permeabilities of the gas and condensate were calculated from the steady-state pressure drops across the core.

Du et al. (2000) developed a method to restore gas relative permeability by injecting methanol into gas-condensate reservoirs. This experiment followed a similar pressure setting approach to that of the experiment of Mott et al. (1999). However, it was noticed that in this experiment, the accumulation of the condensate proceeded sequentially from the inlet of the core to the outlet. The condensate saturation in this study was calculated by measuring the volumes of gas injected and the volumes of gas and liquid produced in the windowed PVT cell. The dynamics of the condensate were reported in this experimental observation, probably for the first time.

These experiments shed light on the measurement of the relative permeability, and are very helpful for understanding the flow behavior in gas-condensate wells. However the number of reported studies relevant to dynamic condensate banking is very limited, and most of the studies did not account for any composition change.

In 2000, Wheaton and Zhang proposed a theoretical model of condensate banking dynamics in an attempt to describe how the compositions of heavy components of a gas-condensate system change with time during pressure depletion. A “Chi” function, defined by the total mobility of component *i* through all phases to the overall mobility of all components in all phases, was found critical in understanding the flow behavior of the condensate bank. It was also noticed that the reservoir permeability and production rate

have significant influence on condensate banking behavior. The composition change of heavy components was found to be rapid in low permeability, high yield reservoirs.

Roussennac (2001) also documented the phase change during the depletion in his numerical simulation. According to Roussennac, during the drawdown period, with the liquid building up in the well grid cell, the overall mixture in that cell becomes richer in heavy components, and the fluid behavior changes from the initial gas-condensate reservoir to that of a volatile oil reservoir. Importantly, since the composition changes with position and time, it is reasonable that wettability, and therefore relative permeability, would also change.

Since the formation and build-up of the condensate is due to the pressure depletion below the dew-point pressure, the near wellbore region, which is characterized by the largest pressure drop, is expected to be the right site of the condensate banking. In this region, a pseudosteady-state flow can be reached at some stage of condensate banking, but a steady-state situation may not be possible considering the composition changes.

This study aims to understand the dynamic process of condensate banking in the near well region from an experimental view. In this research, the manner in which the fluid composition will change with time in the near wellbore region is considered during condensate dropout or revaporization.

Chapter 2 will discuss the flow behavior in gas-condensate systems, and both the phase behavior and condensate banking behavior will be examined. The experimental design based on a laboratory scale simulation will be presented in Chapter 3. According to the parameters from the simulation, the detailed experimental configuration will be introduced in Chapter 4. Chapter 5 and Chapter 6 will present and discuss the experimental results.

Chapter 2

2. Gas-Condensate Flow Behavior

2.1. Gas-Condensate Characterization

Gas-condensates are fluids with unusual behavior between the critical and the cricondentherm temperatures. Between these temperatures, liquid products condense from the gaseous phase. Gas-condensates usually exist in the gaseous state when the initial reservoir pressure is greater than the dew-point pressure of the condensate system. A reservoir fluid is often classified by the shape of the typical phase diagram, but generally, from available production data, several rules of thumb came from the statistical data can all be used to assist in determining the fluid type.

Table 2. 1 shows typical characteristics of condensate, volatile oil and black oil. A more quantitative classification is also given in Figure 2. 1 by using a ternary diagram in terms of mole percent. In the near critical region, gas-condensate has a C_{7+} mole concentration less than 12.5%, while the volatile oil has a higher C_{7+} mole concentration.

Table 2.1: Composition and properties of several reservoir fluids (from CNPC report, 2001).

	Condensate	Volatile oil	Black oil
CO_2 (mol%)	0.53 - 1.94	0.29	0.3
C_1 (mol%)	67.96 - 78.97	51.97	41.3
C_2 (mol%)	6.21 - 6.61	11.72	1.93
C_3 (mol%)	2.37 - 3.22	9.23	3.85
C_4 (mol%)	2.07 - 2.03	4.13	3.67
C_5 (mol%)	1.21 - 1.17	1.82	2.36
C_6 (mol%)	1.47 - 9.92	1.59	3.01
C_7 (mol%)	7.88 - 5.34	17.7	40.58
Mc_{7+}	135-145	185	228
γ_{c7+}	0.7925-0.7734	0.8231	0.8633
T_{Res}(^{0}C)	96.67-102.78	71.67	75.55
P_{sat}(Mpa)	30.5-36.5	28.1	19.7
ρ_{liq}(g/cm^3)	0.2867-0.3668	0.565	

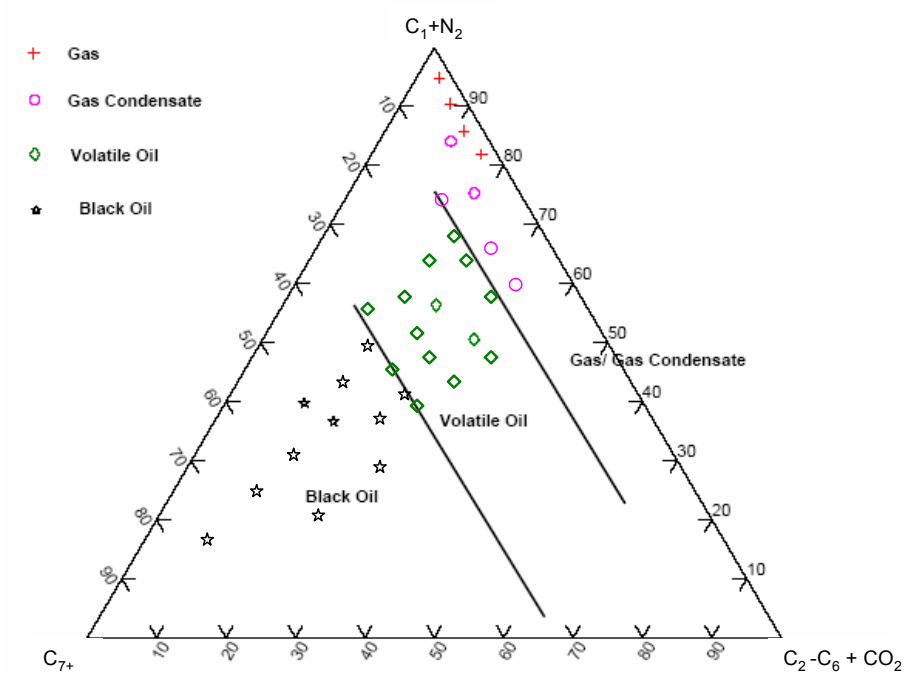

Figure 2.1: Ternary visualization of hydrocarbon classification (from SPE monograph, v.20).

2.2. Gas-Condensate Flow Behavior

2.2.1. Phase and equilibrium behavior

Figure 2.2 is a pressure-temperature diagram for a two-component methane-propane condensate system. The diagram shows that if we have a reservoir pressure at point p_1, the reservoir temperature is located between the critical temperature and cricondentherm temperature, and the reservoir pressure is above the dew-point pressure, so initially the material is totally gas in the reservoir. As pressure goes down from p_1 to p_2 at constant temperature, liquid condenses from the gas to form a two-phase system, and the liquid will not flow until the accumulated liquid reaches the critical condensate saturation.

The reservoir pressure path on the phase diagram (Figure 2.2) suggests that at low pressure, the liquid will begin to revaporize as Figure 2.3 indicates.

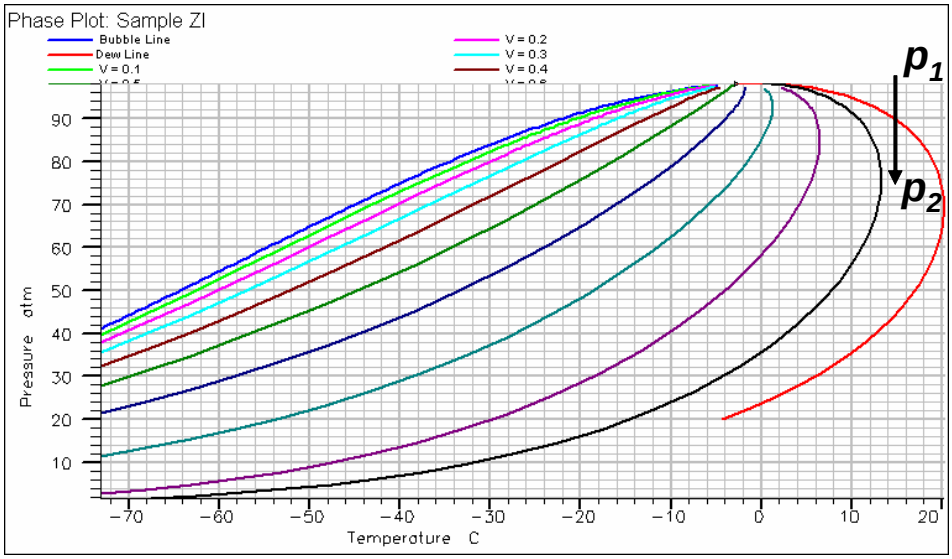

Figure 2.2: Phase diagram of a two-component methane-propane condensate system.

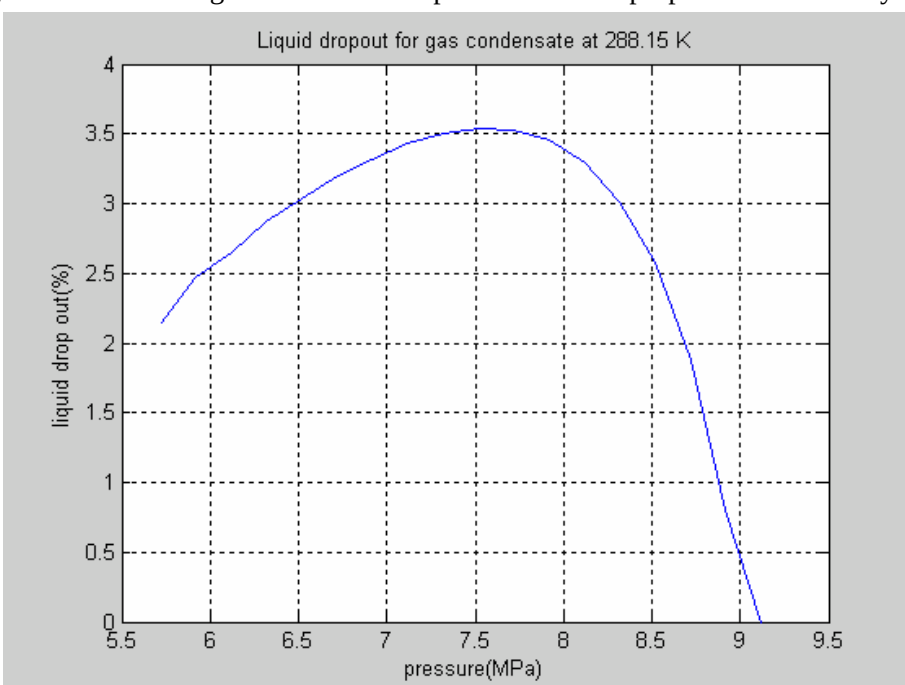

Figure 2.3: Liquid dropout for a two-component gas-condensate system at 15 ^{o}C.

2.2.2. Condensate build up behavior

The three-region theory (Fevang, 1995) has been widely used in literature to characterize gas-condensate flow in the near well region.

The first region (region 3 in Figure 2.4 and Figure 2.5) is the outer part of the reservoir with reservoir pressure greater than the dew-point pressure. In region 3, only a single phase exists.

The second region (region 2 in Figure 2.4 and Figure 2.5) is the middle part of the reservoir with reservoir pressure lower than the dew-point pressure. Liquid starts to drop out in this region, but the condensate is immobile. At this stage, the composition of the flowing gas is becoming leaner as heavier or intermediate components drop out in the liquid phase.

The third region (region 1 in Figure 2. 4 and Figure 2. 5) is the inner part of the reservoir where the pressure drops far below the dew-point pressure. The accumulated condensate saturation exceeds a threshold, the critical condensate saturation, so both the gas and condensate are flowing. Pressure drops in this region at a very rapid rate, hence most of the pressure drop from condensate blockage occurs here, where flow rates are very high.

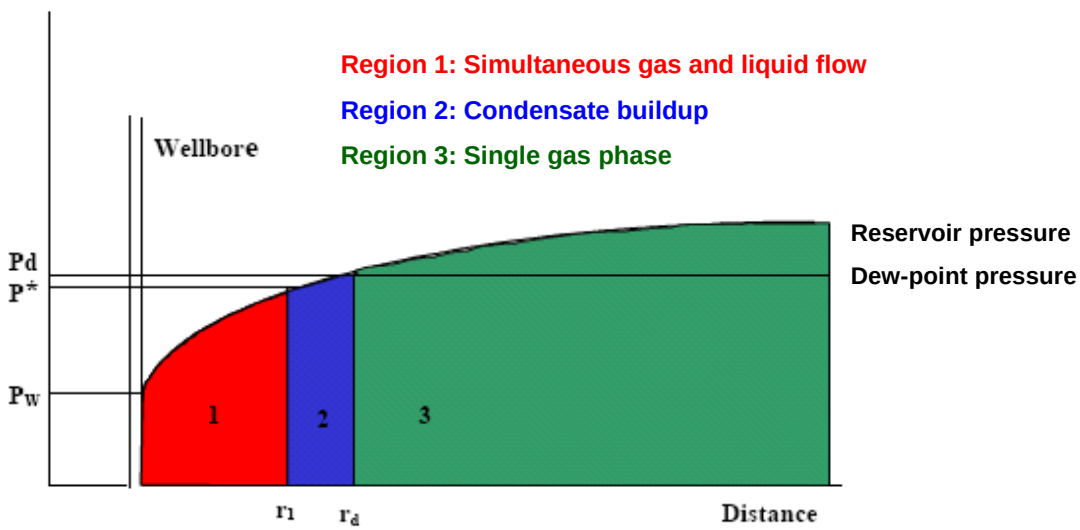

Figure 2.4: Schematic gas-condensate flow behavior.

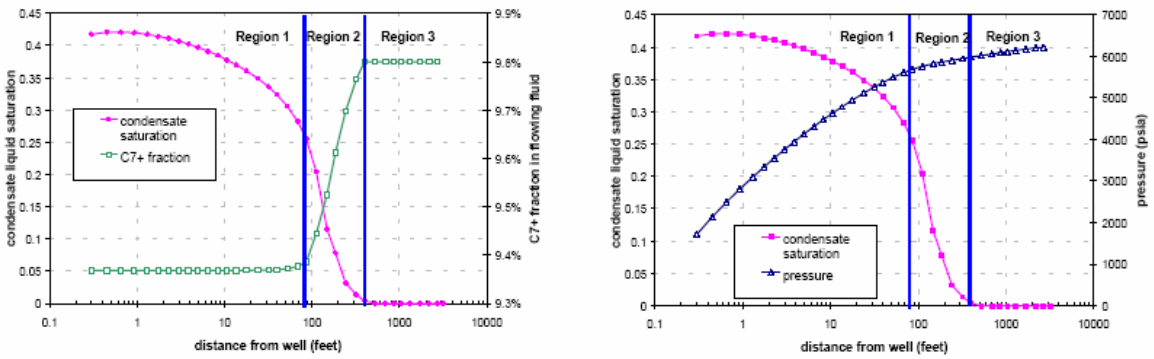

Figure 2.5: Saturation, flowing C_{7+} fraction and pressure versus radius (from Mott, et al. 1999).

2.2.3. Hydrocarbon composition change

In a PVT cell, the overall composition of the whole gas-condensate system will not change during the isothermal pressure depletion, and the liquid drop out would be consist out with the constant depletion curve as indicated in Figure 2.3. However, in a porous medium, the accumulated condensate saturation is much higher than the maximum drop-out from the phase diagram. In reality, the heavier components tend to drop out first and are concentrated in the condensate liquid. The phase diagram of the reservoir fluids is shifted clockwise to a system with higher critical temperature, as in Figure 2.6. In some cases, it is possible that the shifting system has a higher critical temperature than the reservoir, so the reservoir fluid changes from a gas-condensate system to a volatile oil system.

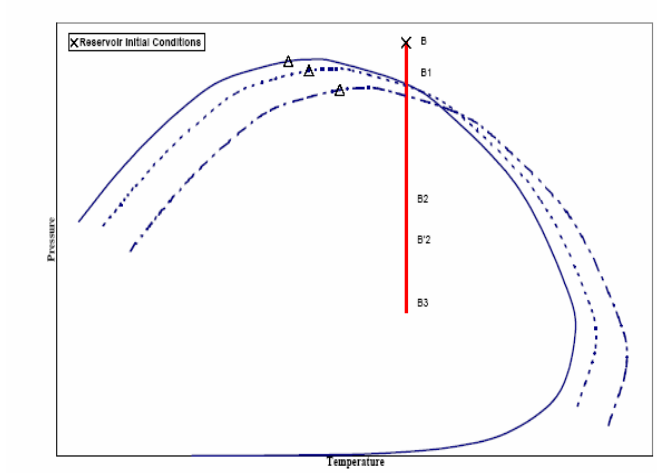

Figure 2.6: Shift of phase envelope with composition change (from Roussennac, 2001).

2.2.4. Relative permeability change

Figure 2.7 shows the input relative permeability curves for the following numerical simulations in this report. These curves are typical for gas-condensate systems. This figure indicates that once the accumulated condensate saturation is greater than the critical gas-condensate saturation (S_{cc}), effective gas permeability experiences dramatic decreases. In regions far away from the wellbore the condensate accumulation has also reduced gas relative permeability, but this is generally a second order or negligible effect.

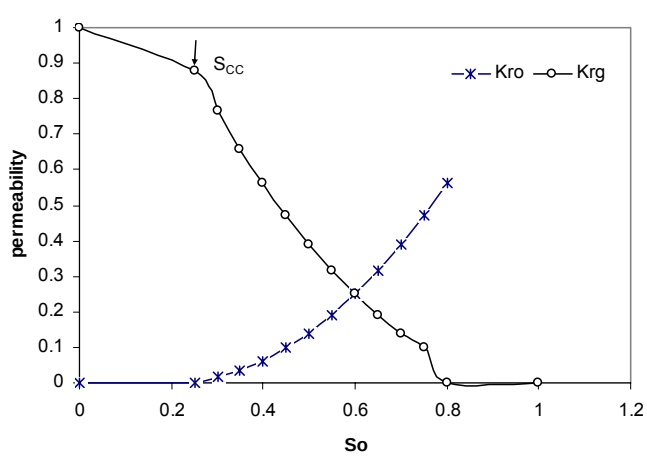

Figure 2.7: Input relative permeability curves for numerical simulation.

Chapter 3

3. Experimental Design

A two-component methane-butane gas-condensate system (Figure 3.1) was used in this experiment. Components designed for the synthetic system are based on the following principles: first, they should be easy to handle, thus two to four components are preferred; second, critical temperature and pressure of the system should not be too high; third, a broad condensate region is desirable in order to achieve a reasonable condensate saturation and experimental duration; finally, gas and liquid should show a large discrepancy in density so as to be easily distinguished in the X-ray CT scanner. Figure 3.1 shows the phase envelope for a gas-condensate system with 85% methane and 15% butane gas condensate system. At temperature of 20 °C and the pressure from 125 atm to 75 atm, this phase diagram gives a good retrograde region.

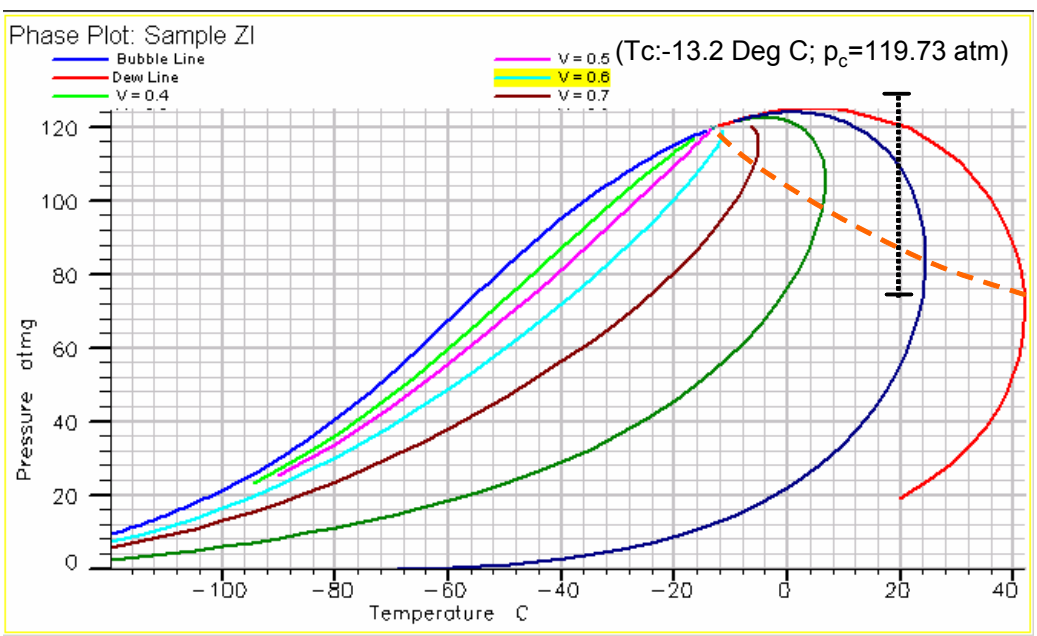

Figure 3.1: Phase diagram for the methane-butane system.

3.1. Laboratory scale simulation

To ensure this choice of fluid system can give the reasonable condensate saturation and experimental duration, two simulations were investigated: a draw-down flow test and a constant pressure-drop flow test. In both cases, the linear flow option in Eclipse 300 was used to simulate the gas flowing through a Berea sandstone core plug. The core plug is in cylindrical with length of 25.4cm and diameter of 5.06cm. The average porosity for this core is 15% and the permeability 2.1md.

For simulation in the linear direction, the cylindrical core was approximated with Cartesian grid blocks in the X, Y and Z directions. Since the flow is only in the X direction, the numbers of grid blocks in Y and Z directions are both one. A virtual grid block was set to simulate the injection well in the depleting reservoir. The size of this grid block in the X direction was set to 2cm and the porosity to 100%, hence, this virtual grid could provide the injection well with a total fluid capacity of 4021.8 cm^3.

The production well produces at constant bottomhole pressure of 75atm. The difference in the manner of injection separates the two test simulations. The draw-down test has no control of the injection well, as the reservoir pressure keeps dropping during the depletion process until the whole reservoir pressure reaches 75 atm (see Figure 3.2), while for the constant pressure drop test, the injection well injects at a constant pressure 125 atm, hence, the reservoir will produce under constant pressure drop condition (Figure 3.11).

3.1.1. Draw-down test simulation

For the draw-down test simulation, the production pressure was first fixed at 75 atm, the test lasted for 20.825 hours and the major saturation and composition changes happened within the first 0.325 hours (19.5 minutes), this pressure set gave a manageable experiment duration. Figure 3.3 shows the saturation profile at different time steps. As expected, the condensate drops out first in the near well region, and then propagates towards the injection well. The condensate saturation increases at first as the condensate

accumulates in the core plug as the pressure goes through the retrograde region. After the pressure passes the maximum condensate drop-out region, the condensate saturation starts to drop until a final stabilized saturation, where the condensate is stuck in the core.

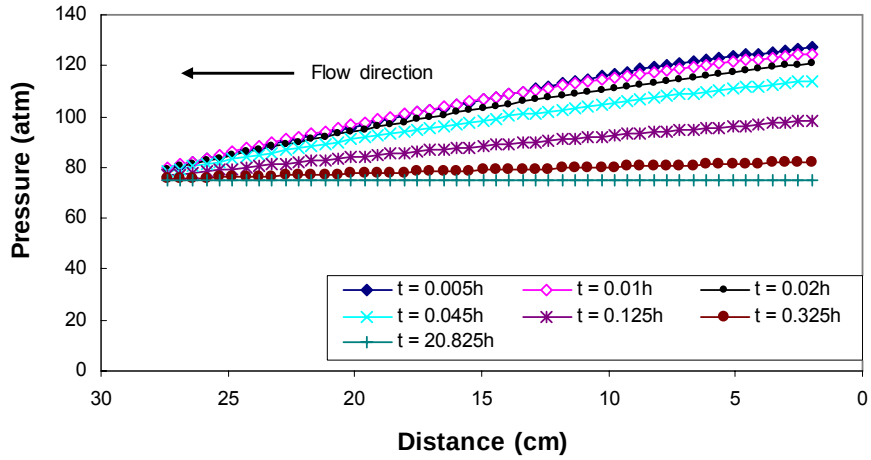

Figure 3.2: Pressure profile for draw-down test simulation.

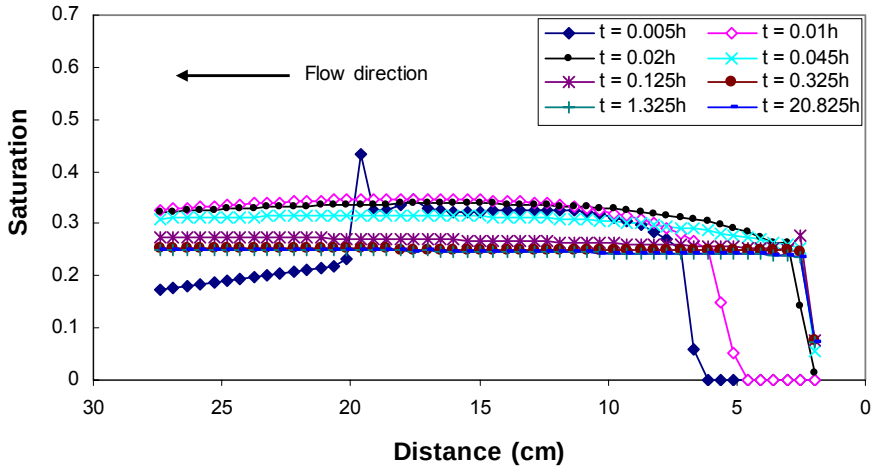

Figure 3.3: Saturation profile for draw-down test simulation.

As the gas flows through the core, the heavier component, in this case butane, drops to the liquid phase, and butane becomes leaner and leaner in the flowing phases (gas phase and the mobile liquid phase). This is confirmed by the Figure 3.4, and from this figure, we also noticed that in the near well region, the butane mole fraction drops to a low value very quickly.

Figure 3.6 shows the density difference between vapor and liquid phases. The density of the liquid phase is greater than 0.35 in most cases, and the vapor density below 0.2 in general. This density difference can be distinguished in the CT scanner.

For different production pressure, the simulation results show that the lower the pressure of the production well, the lower the final stabilized condensate saturation. If this can be confirmed in the experiment, then the condensate saturation stuck in the reservoir can be controlled by simply applying a specific bottomhole pressure to the production well.

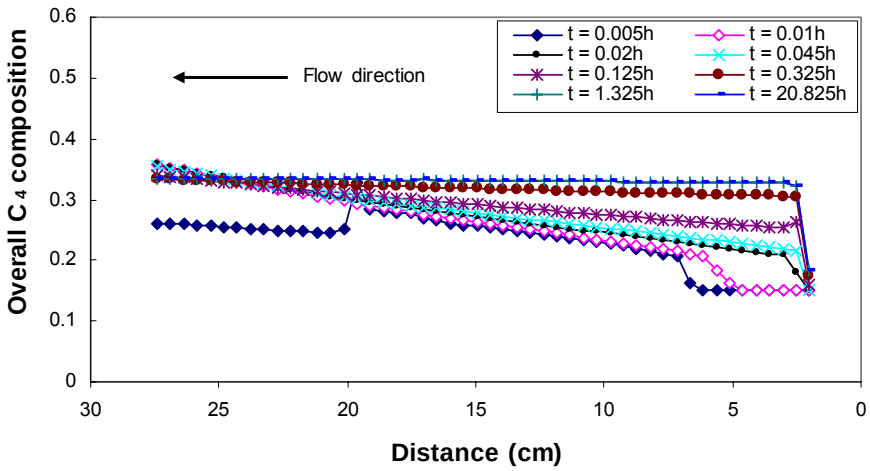

Figure 3.4: Overall C_4 composition change for draw-down test simulation.

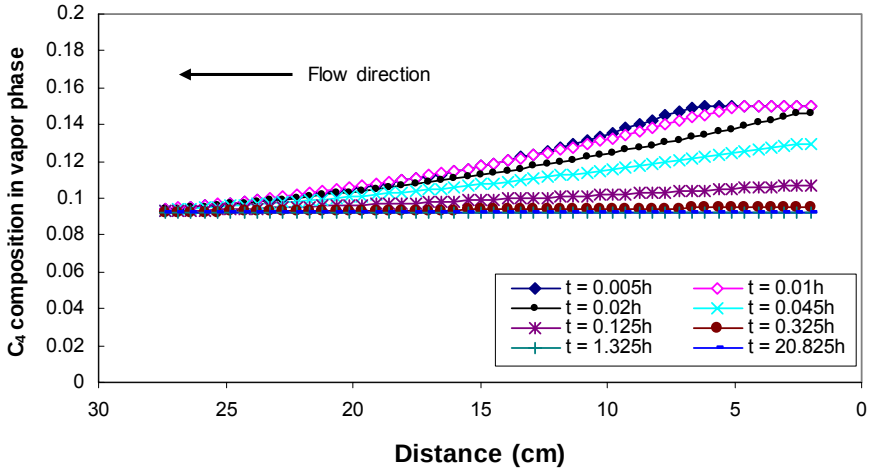

Figure 3.5: C_4 composition profile in vapor phase for draw-down test simulation.

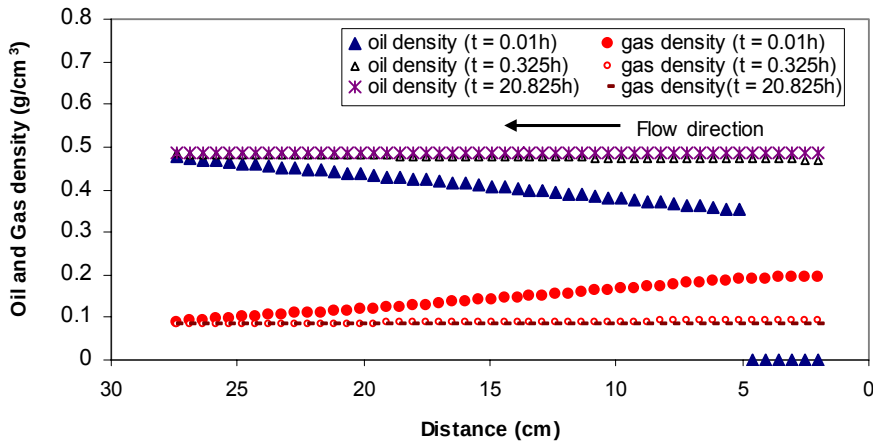

Figure 3.6: Density profile for draw-down test simulation.

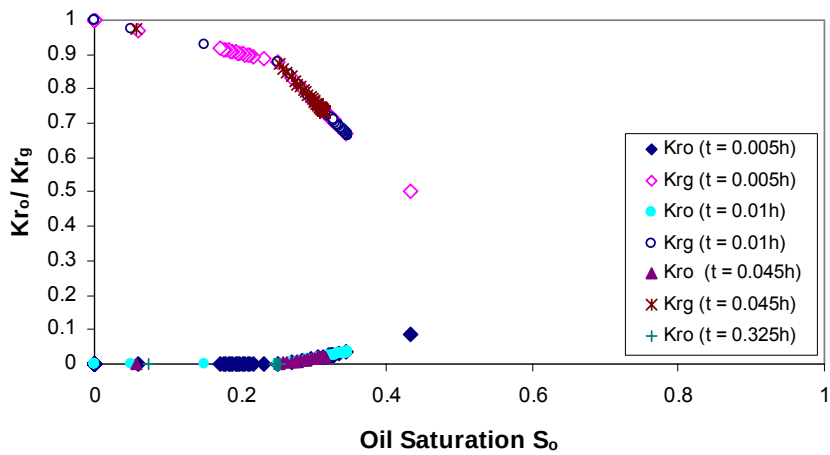

Figure 3.7: Draw-down test relative permeability curves.

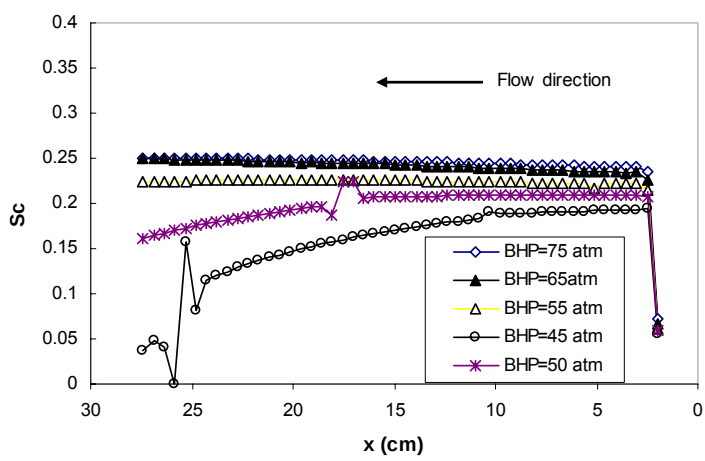

Figure 3.8: Saturation profile at different bottomhole pressure (BHP).

The heavier component tends to increase in the grid cell as the production well BHP decreases (Figure 3.9), and the increase in the heavier components in the grid cell gives the lower condensate saturation (Figure 3.10).

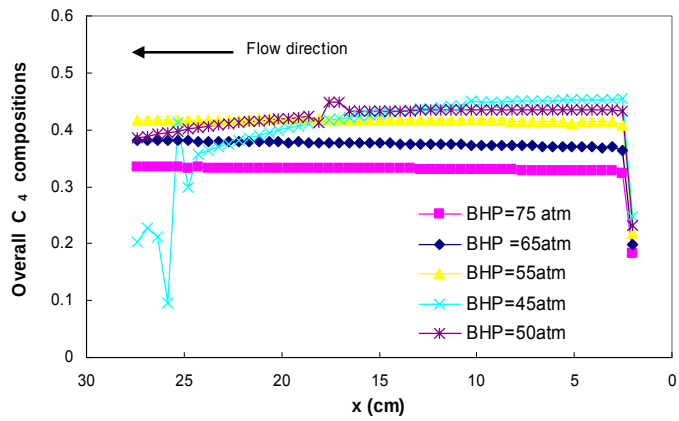

Figure 3.9: Composition profile at different bottomhole pressure (BHP).

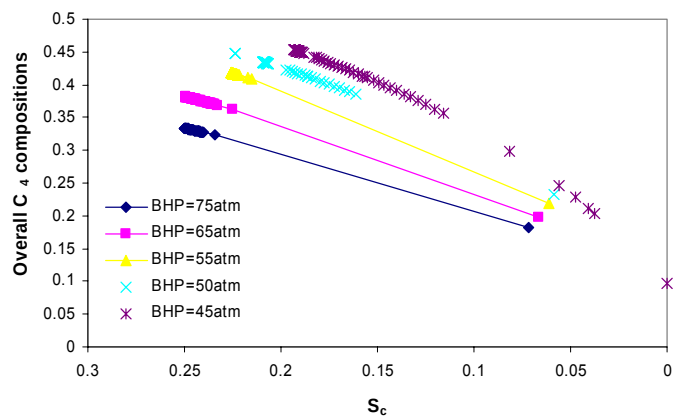

Figure 3.10: Overall C_4 composition vs. S_c.

3.1.2. Constant pressure-drop test simulation

It was observed from the constant pressure-drop simulation that the heavier component experiences a large composition variation along the X direction (Figure 3.13) since the pressure difference along the neighbor grids is constant, unlike in the draw-down test.

From the experimental view, the composition change in this case would be easier to observe.

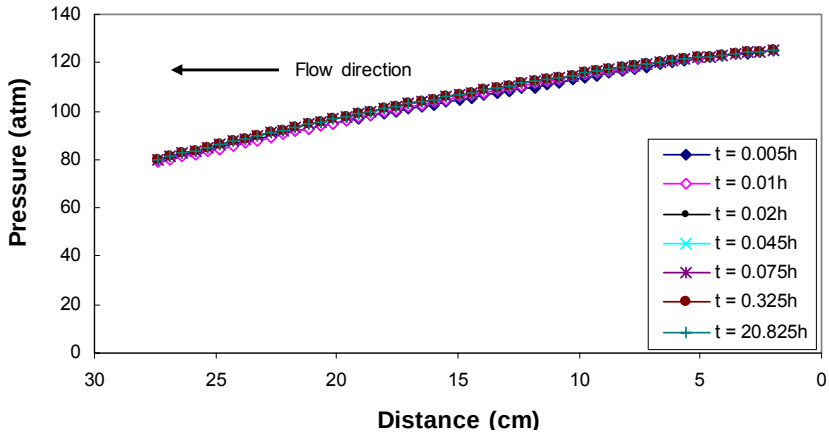

Figure 3.11: Pressure profile for constant pressure drop test simulation.

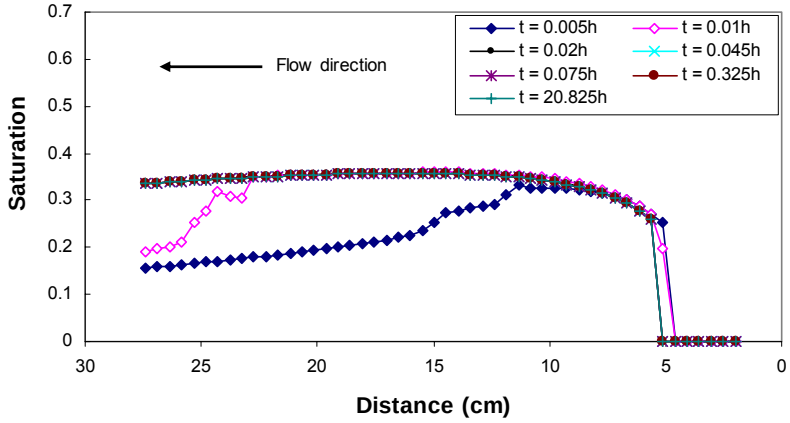

Figure 3.12: Condensate saturation profile for constant pressure drop test simulation.

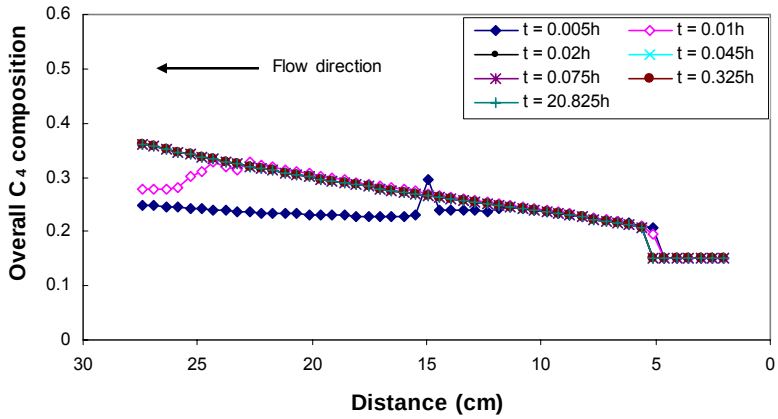

Figure 3.13: Overall C4 composition profile for constant pressure drop test simulation.

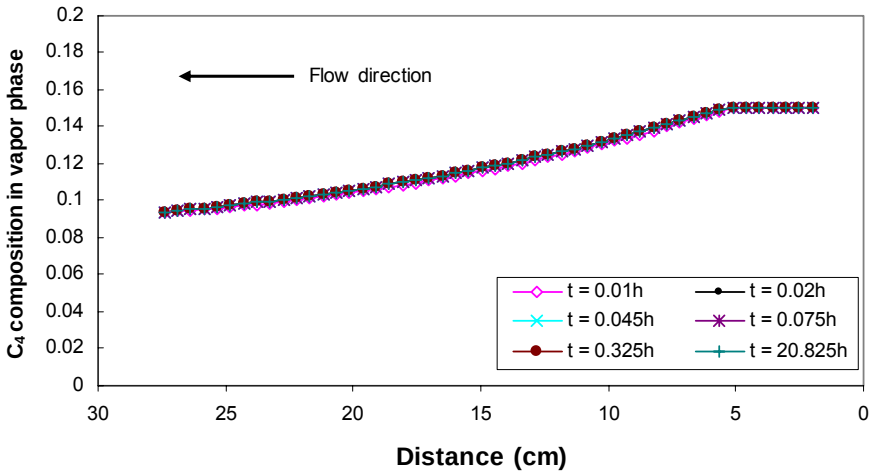

Figure 3.14: C_4 in vapor phase profile.

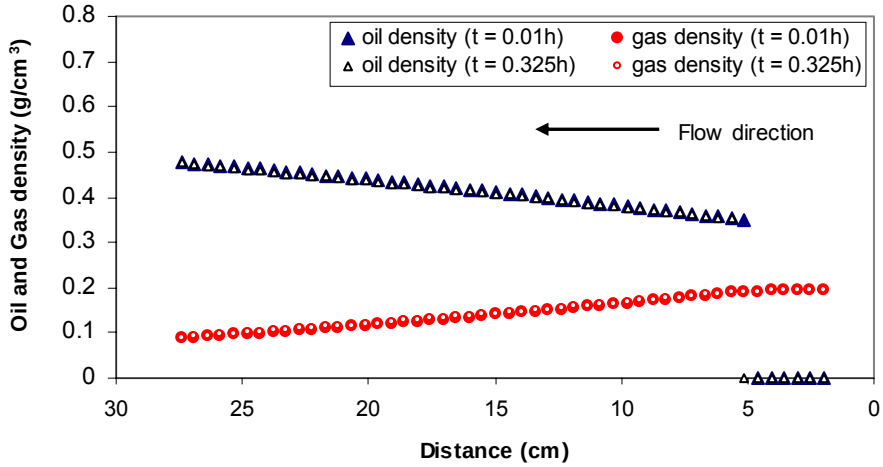

Figure 3.15: : Density profile for constant pressure drop simulation.

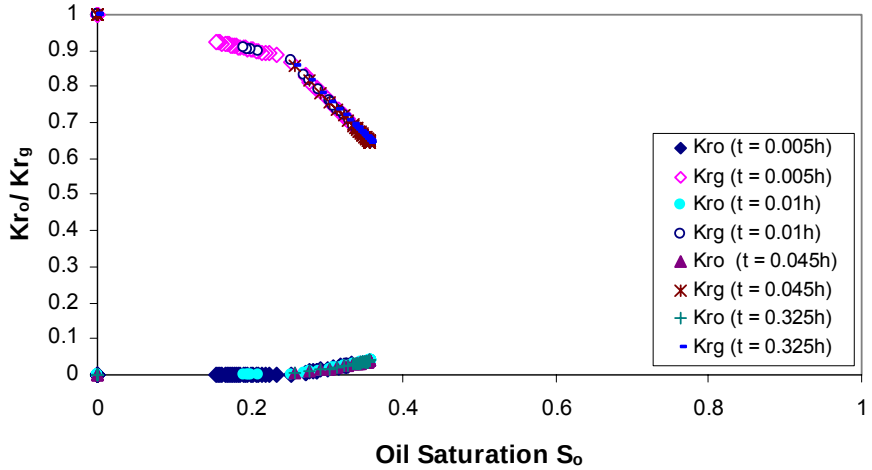

Figure 3.16: Constant pressure drop test relative permeability curves.

3.2. Experimental design

3.2.1. Difference between static values and flowing values

To design the experiment based on the simulation results, it is important to understand the difference between static and flowing parameter values first. The static values are at a given reservoir location, while the flowing values are only associated with the property of the flowing fluids at this given location and a given time. In reservoir simulation, static values will refer to the property values of a given grid block at a given time, while in the experiment and real field cases, the sample only comes from the flowing phase. Hence, the measured heavier composition will be always less than the simulation values (see Figure 3.17).

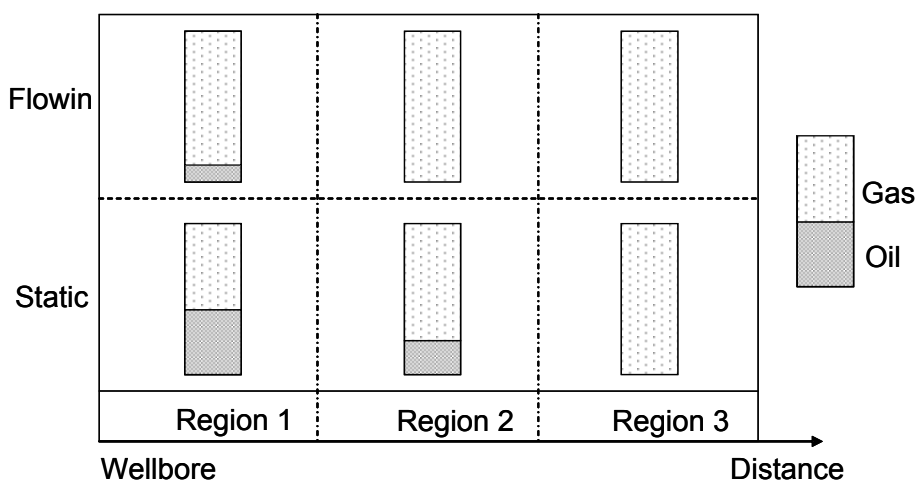

Figure 3.17: Schematic diagram for static and flowing values.

3.2.2. Experimental design

From the simulation results for both the draw-down simulation and the constant pressure drop test, we can see that the duration of the major change in composition and saturation is about 19 minutes, which is manageable under experimental conditions, and the density difference in both cases is greater than 0.15, which is distinguishable in the CT scanner.

Both simulations were run at room temperature (20°C) and at pressure less than 130 atm, which can be controlled in the laboratory easily, so a gas mixture of 85% methane and 15% butane was proposed for the experiment.

Chapter 4

4. Experimental Procedure

4.1. Experimental Apparatus Description

The gas-condensate flowing system consists of four major parts (see Figure 4.2): the gas supply and exhaust part, the core flow system part, the gas sampling part, and the data acquisition part.

The upstream gas mixture was stored in a piston cylinder (Hai An, China, capacity 4,000 ml, pressure range 0-32 MPa), which was attached to a water pump (HIP, model 62-6-10). This was to control the gas supply pressure to make it higher than the gas-condensate dew point pressure. The downstream gas exhaust was discharged to the hood directly for this experiment since the total volume of the exhaust is small. For a larger volume exhaust, a piston cylinder on the downstream side may also be used to store the exhaust, which can also be recycled for future experiments.

The core flow system part consists of the titanium core-holder (Shiyi Science and Technology, model J300-01), which can support a system pressure as high as 40 MPa, and a Berea sandstone core plug with length of 25.04 cm and diameter of 5.06cm.

The gas samples were collected into seven Tedlar gas sampling bags (SKC west, model 232-02), six along the core-holder and one at the downstream port for the exhaust gas. Gas sampling bags were connected to the system in a way that the bags can be vacuumed before the experiment and the sampling gas pressure is low enough not to burst the bags (see Figure 4.1 gas sampling part). Since the pressure regulator is not small enough to be fitted into the sampling system, seven check valves (Swagelok, model SS-2C-25) with 25 psi output pressure have been used to relieve the excess flowing pressure at the sampling tape to 25 psi before the gas enters the sampling bags. Gas flow through the check valves was passed through the stainless tubing and into the exhaust tank at the end.

An HP 5880A series gas chromatograph was used to analyze the composition of gas samples. A 30 feet packing column (Alltech, model 12713) was specified for the TCD detector for the light component analysis.

Different capacity pressure transducers were used to measure the absolute pressures and the pressure drops occuring during the gas flowing process. Two 2,000 psi transducers were attached to the core-holder inlet and the first sampling port to measure the upstream flowing pressure of the system and the core plug respectively. Experience showed that the pressure drop between the core-holder inlet and the first core port is very small, hence the original mixture entering into the core plug was ensured to be above the dew-point pressure. Two 1,250 psi transducers were attached to the end of the core-holder and the last sampling ports. Figure 4.1 shows the experimental pressure drops for different flow pressures along the core-holder, pressures at X = 40cm and x = 48cm are corresponding to the pressures at the last sampling port and the end of the core-holder respectively. From this figure, we can see that pressure shows a higher drop in the downstream part of the flow. Hence, to achieve a 75 atm pressure at the end of the core plug, we should specify a low pressure at the end of the core-holder. Pressure differences along the sampling ports were measured by the 320 psi transducers.

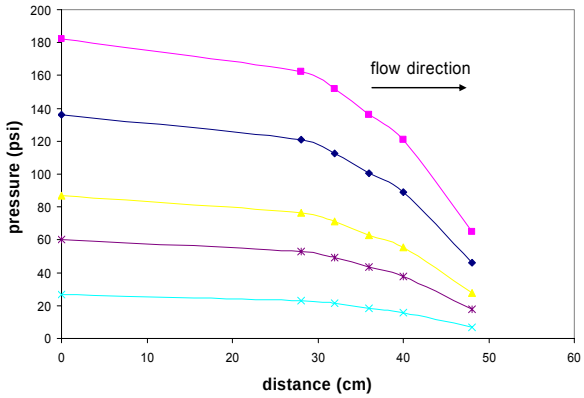

Figure 4.1: Pressure drop along the core-holder.

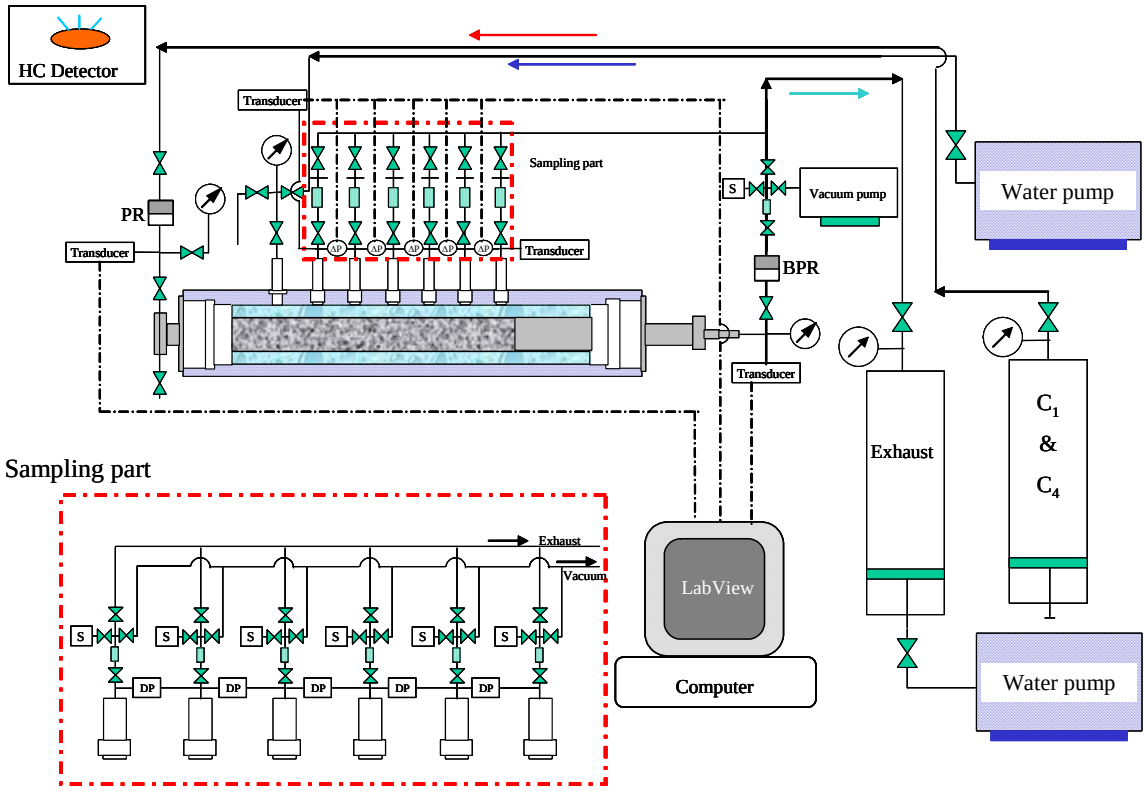

Figure 4.2: Schematic diagram of the gas condensate flow system.

4.2. Gas System

According to the simulation design, 5.5847mole butane and 31.6465mole methane were required to fill in the piston cylinder with size of 3,920ml at 2000 psi and give the component composition of 85% methane and 15% butane.

5.6 moles of liquid butane was first transferred to the piston cylinder as shown in Figure 4.3. The butane supply cylinder has a pressure of 60 psi, which is higher than the vapor pressure of butane at room temperature; hence the butane in the cylinder is in the liquid phase. The butane cylinder was put upside down such that the liquid butane can flow directly into the piston cylinder, and drive the prefilled water out from below the piston. The mass of the butane transferred was then calculated through the volume measurement of the water discharged from the piston cylinder.

The maximum pressure of the methane supply cylinder was 2000 psi. Methane was transferred directly to the piston cylinder (Figure 4.4), which already had 5.6 moles of butane inside. The pressure of the piston cylinder with butane was only 43 psi, so the methane flowed into the piston cylinder by the large pressure difference between the methane supply and the piston cylinders. After fully mixing and equilibrium, the final mixture had a pressure of 1,800psi. The gas chromatograph (GC) results indicated that component composition of the mixture was 81% methane and 19% butane under pressure 1,800 psi. The mixture was pressurized to 2,350 psi prior to the gas flow experiment.

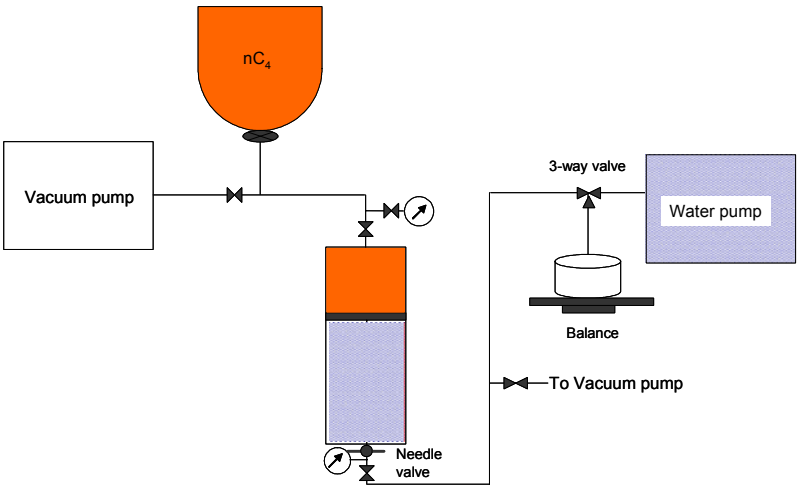

Figure 4.3: Schematic diagram for Butane (C_4) transfer process.

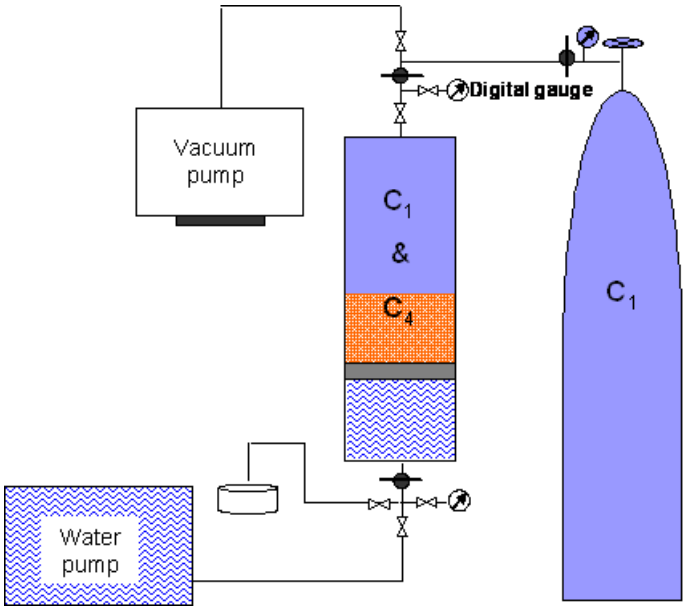

Figure 4.4: Schematic diagram for Methane (C_1) transfer process.

4.3. Experimental Procedure

The experimental apparatus and data acquisition system were both tested with nitrogen before the main experiment. Experience with nitrogen flushing showed that some of the differential pressure transducers had zero shifts as the system pressure increased. Due to this unsteady nature, the pressure transducers were recalibrated under a system pressure as high as 1,800 psi, and the measuring error was also analyzed before the hydrocarbon experiment.

4.3.1. Pressure transducer calibration

Figures 4.4-4.10 show the calibration results for nine transducers, all showing good linear relationships when the transducer experienced single-sided pressurization. For the upstream and downstream absolute pressure measurements, these calibration results satisfy the measuring requirement. Three differential pressure transducers (transducers 2, 3 and 4) showed zero shifting from -2.5 – 3 psi when the system pressure increases to 1,200 psi. Pressure measurements under both-side pressurization (Figure 4.14) show that the measuring error is within ± 1 psi when the pressure difference in the range of 70-150 psi. For this experiment, the total constant pressure drop along the core-holder is 50 atm, the average pressure difference along every two sampling tapes is 10 atm (147 psi), hence the measuring error did not influence the measuring results significantly.

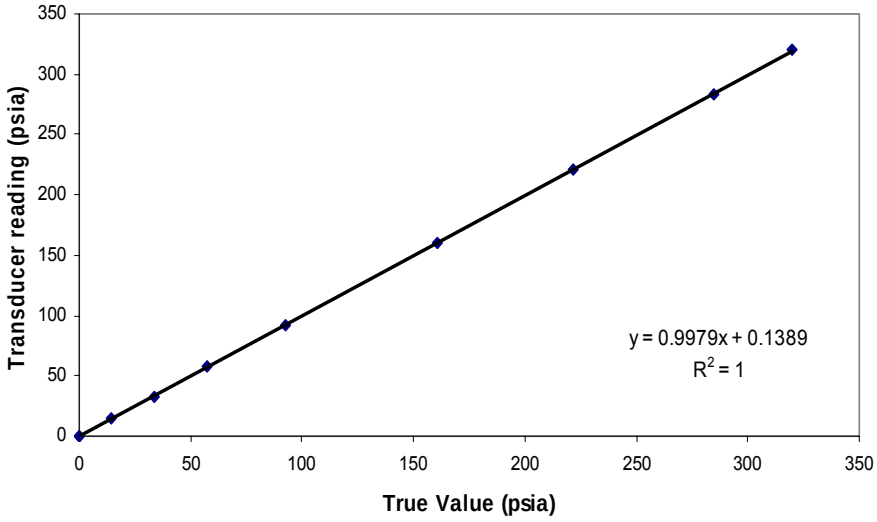

Figure 4.5: Pressure transducer 1 calibration.

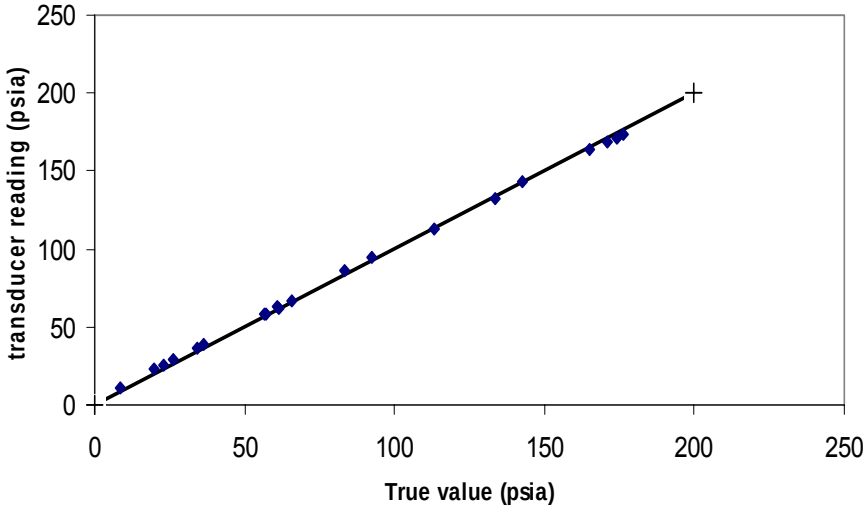

Figure 4.6: Pressure transducer 2, 3 and 4 calibration.

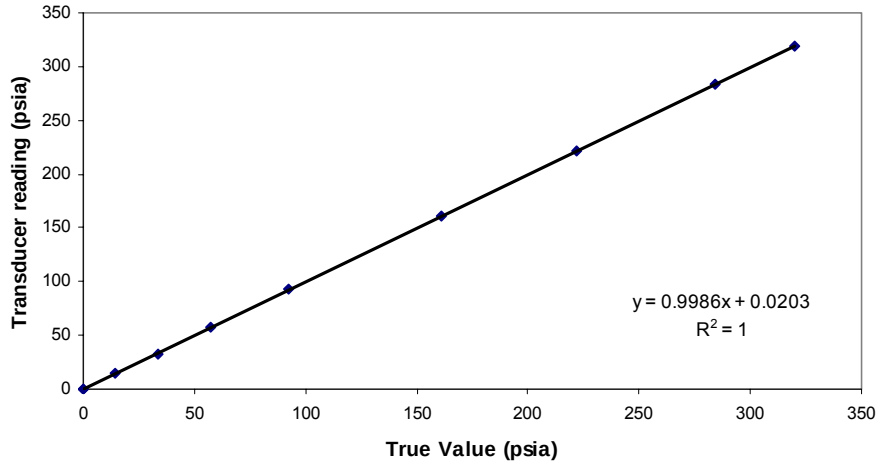

Figure 4.7: Pressure transducer 5 calibration.

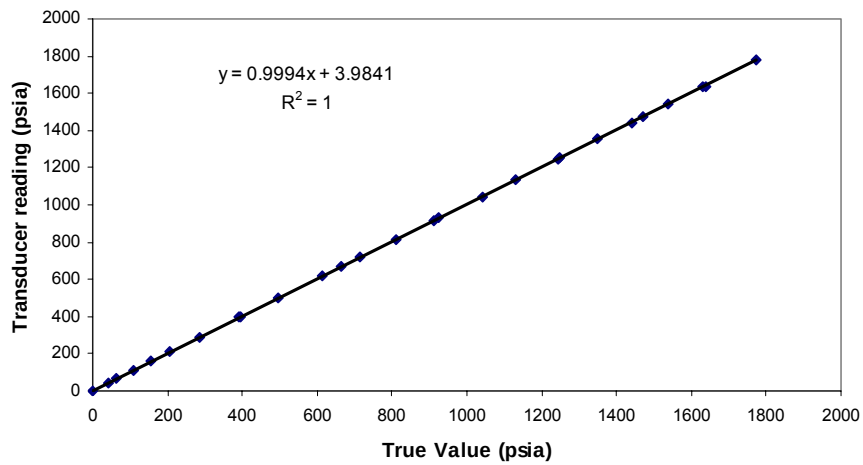

Figure 4.8: Pressure transducer 6 calibration.

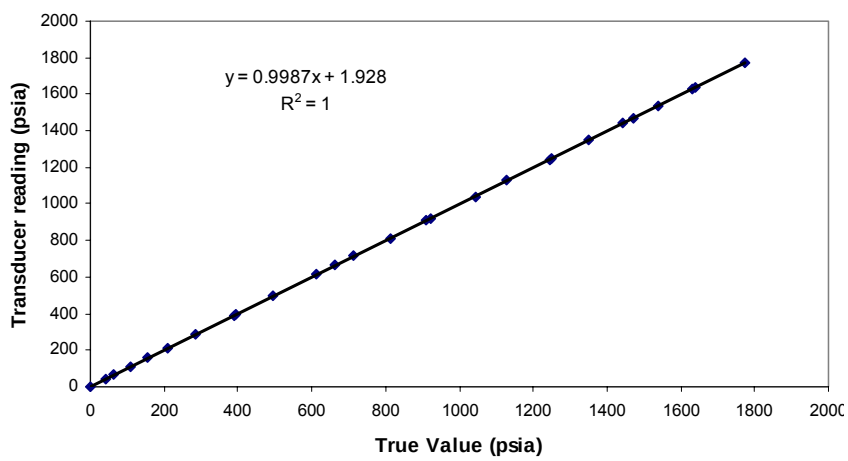

Figure 4.9: Pressure transducer 7 calibration.

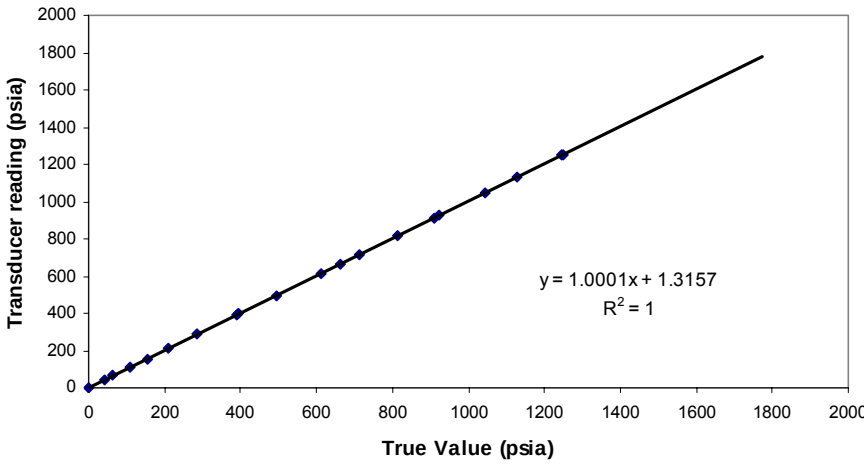

Figure 4.10: Pressure transducer 8 calibration.

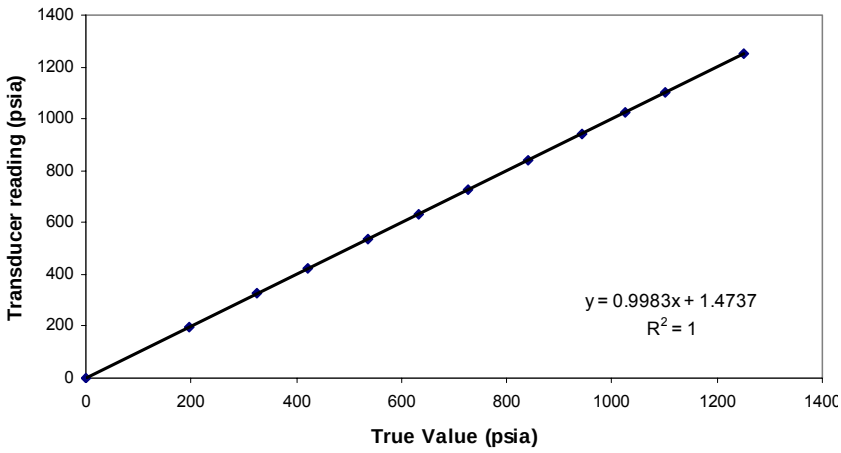

Figure 4.11: Pressure transducer 9 calibration.

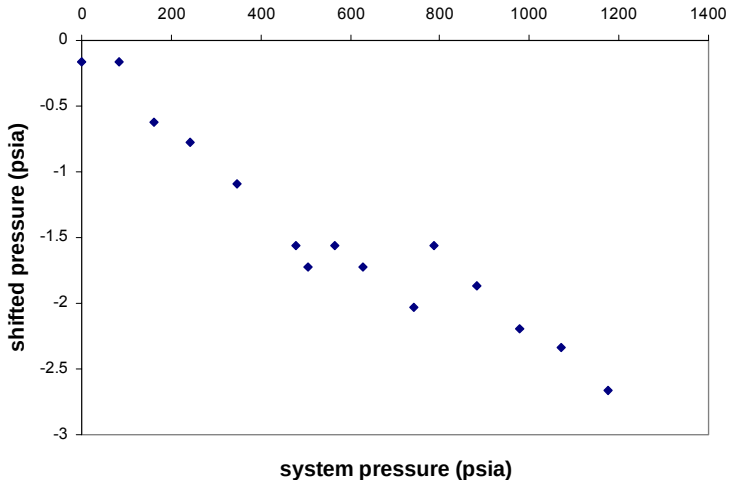

Figure 4.12: Zero shift tests for pressure transducer 2.

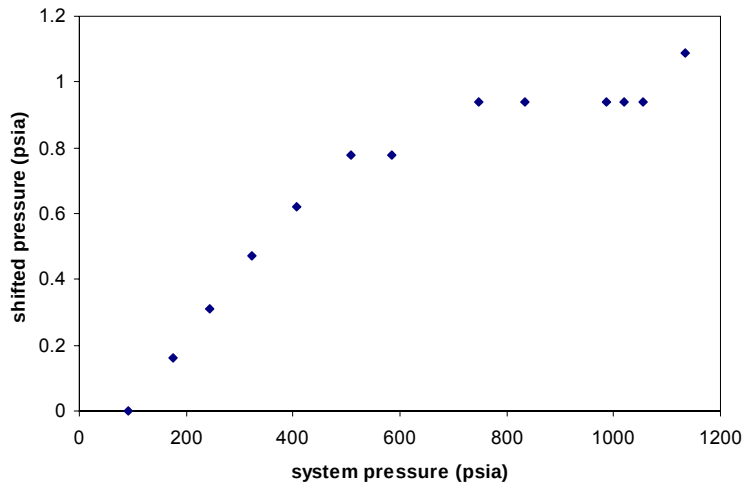

Figure 4.13: Zero shift tests for pressure transducer 3.

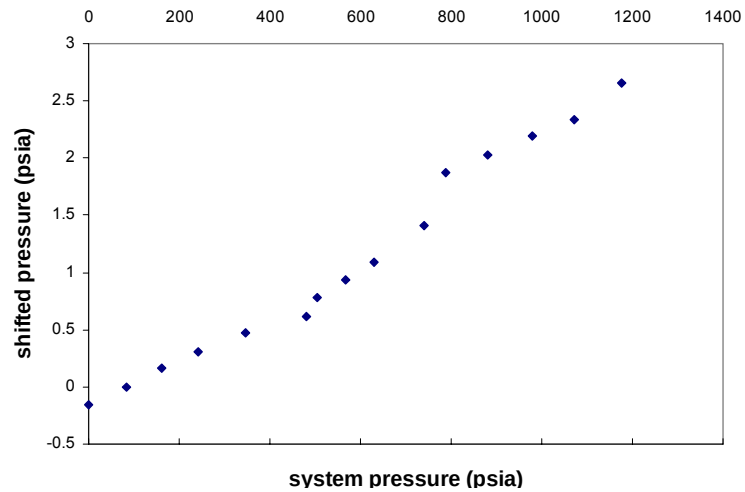

Figure 4.14: Zero shift test for pressure transducer 4.

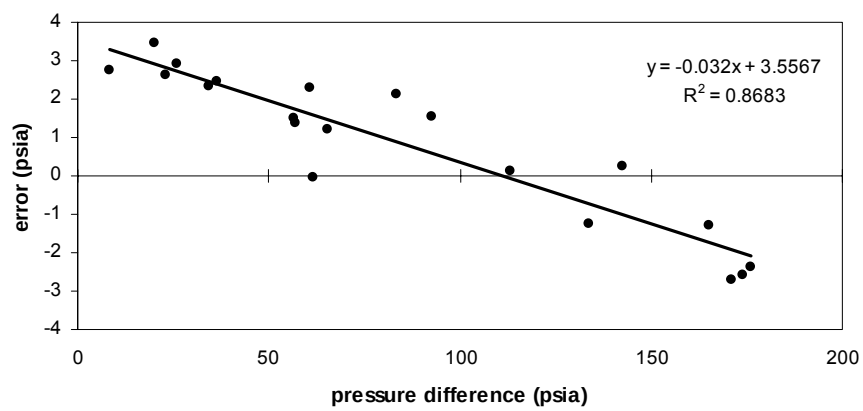

Figure 4.15: Measuring error under different pressure difference.

4.3.2. Gas Sampling

Three major flow tests were performed during the experiment. Before the flow test, the core was saturated with pure methane at a pressure of 1,806 psi, the maximum pressure that the methane supply cylinder could provide. Then about 1-2 pore volumes of gas mixture of methane and butane (as described in Section 4.2) was flushed through the core. The dew point pressure of this gas mixture was 1,890 psi (128.6 atm) at room temperature 21°C, hence when the mixture flowed into the core system at pressure 1,806 psi, some condensate could have dropped out in the core. The core system pressure after equilibrium was 2,106.8 psi. The first batch of gas samples along the core was taken at this condition, and after the sampling the average core pressure dropped slightly to 2,000 psi. All six sample ports were opened and closed simultaneously to ensure that the samples were taken at the same time. In some cases, the sample size was not large enough for gas chromatograph (GC) analysis, so we reopened the valves between the sample ports and the core-holder one by one to capture more sample volume. Samples collected in this case may be slightly different from those taken simultaneously.

The first flow test was achieved by adjusting the upstream pressure regulator (Go company, model BP57-1A11C2N147) and the downstream back-pressure regulator (Go company, model BP66-1B11CJN15F). After the upstream and downstream pressures reached 1,625.6 psi and 1,200 psi respectively, the second batch of gas samples were taken simultaneously along the core-holder. The same procedure as in the first batch sampling process was followed.

In the second flow test, the gas mixture supply had been shut down. The gas mixtures blew through the core system until the upstream pressure dropped to 663.09 psi. Seven samples were collected in this test run, six along the core-holder and one from the exit port. The upstream pressure was further decreased in two steps to 500 and 191 psi, and another two gas samples were taken at the exit at each step.

The third flow test was similar to the second except that the upstream pressure was further drawn down to 61.5 psi. Only two samples were taken along the core due to the small volume of gas in the core system and one final gas sample was taken at the exit.

All gas samples were collected in the sampling bags and sent to the gas chromatograph for composition analysis.

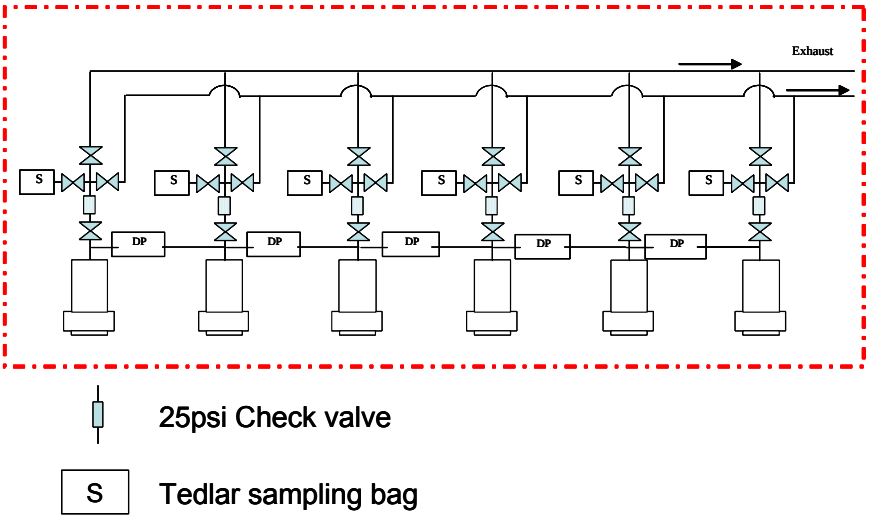

Figure 4.16: Schematic diagram for gas sampling part.

Chapter 5

5. Results and Discussion

5.1. Composition Changes

Table 5.1 shows the gas chromatograph results for all the gas samples. Notice that the first batch of gas samples, which were collected before the flow test, show different composition for the same component (C_1 or C_4) at different sample ports and these compositions also differ from the initial compositions. The samples taken at the sample port 2 and 6 are the only two samples exactly equal to the initial compositions. Sample 1, 3 and 4 show higher C_4 percentage and sample 5 shows lower C_4 percentages compared to the initial 19% C_4 percentage. This may be due to the fact that the core was presaturated with pure methane at pressure 1,800 psi, which is lower than the dew point pressure (1,890 psi) of the initial gas mixture. When the high pressure gas mixture (2,135 psi) flowed through the lower pressure core, some condensate drops out nonuniformly in the core.

When the upstream pressure drops, more gas condensate drops out into the core, and the accumulated the condensate liquid, which is richer in heavier component, can not flow until the condensate saturation reaches threshold saturation. Hence the flowing phase consists of lighter component; this is confirmed by the composition increment in C_1 component in the second and the third flow test. Notice that the composition distribution trends for the second and the third flow test follow the first one; all have low heavier composition percentage at sample port 5 and high C_4 percentage at the sample port 4.

When the core system pressure drops below the pressure corresponding to the maximum liquid drop-out point, the condensate starts to revaporize, a high percentage of heavier component was expected to be seen at this stage. This is also confirmed by the

composition results from the last batch samples, where the sampling pressure was only 61.5 psi and the C4 composition is as high as 57.5%.

Results from the exit samples are consistent with the samples taken from the core system except for the first sample, which was taken at pressure 663.1 psi. A possible reason is that it was the first sample taken at the exit, the liquid drop-out accumulated along the sample port during the previous experiment was also flowed into the sample bag, so the sample had more of the heavier component (20.2% C_4) compared with average 11% C_4 from the core samples.

Table 5.1: Component composition results from GC analysis.

	Port #	upstream pressure (psi)	downstream pressure (psi)	C_1(%)	C_4(%)
1st batch	1	2,016.8	2,016.8	75.7059	24.2941
	2	2,016.8	2,016.8	79.9017	20.0983
	3	2,016.8	2,016.8	78.3106	21.6894
	4	2,016.8	2,016.8	75.4468	24.5532
	5	2,016.8	2,016.8	84.2324	15.7676
	6	2,016.8	2,016.8	81.5232	18.4768
2nd batch	1	1,625.5	1,200.0	85.1364	14.8637
	2	1,625.5	1,200.0	85.8917	14.1083
	3	1,625.5	1,200.0	85.7908	14.2092
	4	1,625.5	1,200.0	81.4240	18.5760
	5	1,625.5	1,200.0	88.8917	11.1084
	6	1,625.5	1,200.0	89.4812	10.5188
3rd batch	1	663.1		90.6191	9.3809
	2	663.1		89.0813	10.9187
	3	663.1		89.0747	10.9253
	4	663.1		87.7008	12.2992
	5	663.1		89.1545	10.8455
	6	663.1		90.0530	9.9470
4th batch	1	61.5		47.3548	52.6452
	2	61.5		42.4955	57.5045
Exit port	1	663.1		79.8133	20.1868
	2	500.0		83.9280	16.0720
	3	191.0		50.9252	49.0748
	4	61.5		40.9915	59.0085

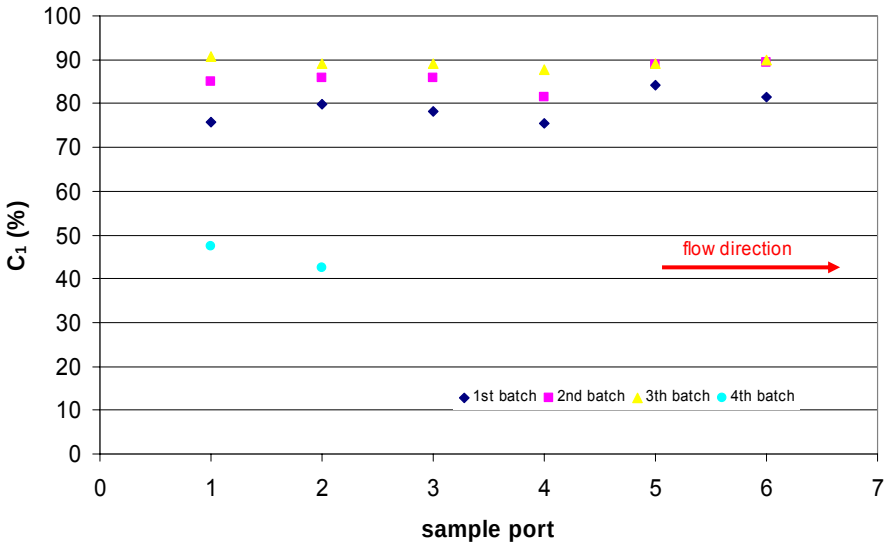

a). Methane compositions.

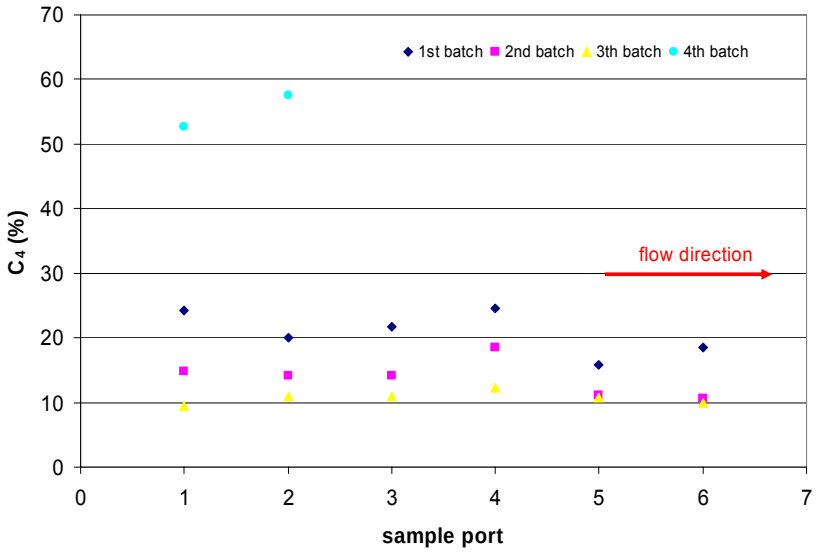

b). Butane compositions.

Figure 5.1: Component compositions for different experimental tests.

5.2. Nitrogen Permeability Changes

Nitrogen permeability was measured before and after the hydrocarbon flow test. Figure 5.2 shows the results during different times. From the figure, we can see that permeabilities measured right after the hydrocarbon flow test are lower than those measured before the test, which indicates the possibility of unevaporated liquid drop-out inside the core. The fact that liquid appeared still to be present even though the original phase diagram would have predicted complete revaporization is of primary importance, as it shows that the liquid remaining in the core was not of the same composition as the original.Nitrogen permeability measured two weeks after the hydrocarbon flow test is consistent with those measurements before the hydrocarbon flow test, which confirmed the ultimate revaporization of the condensate in the core.

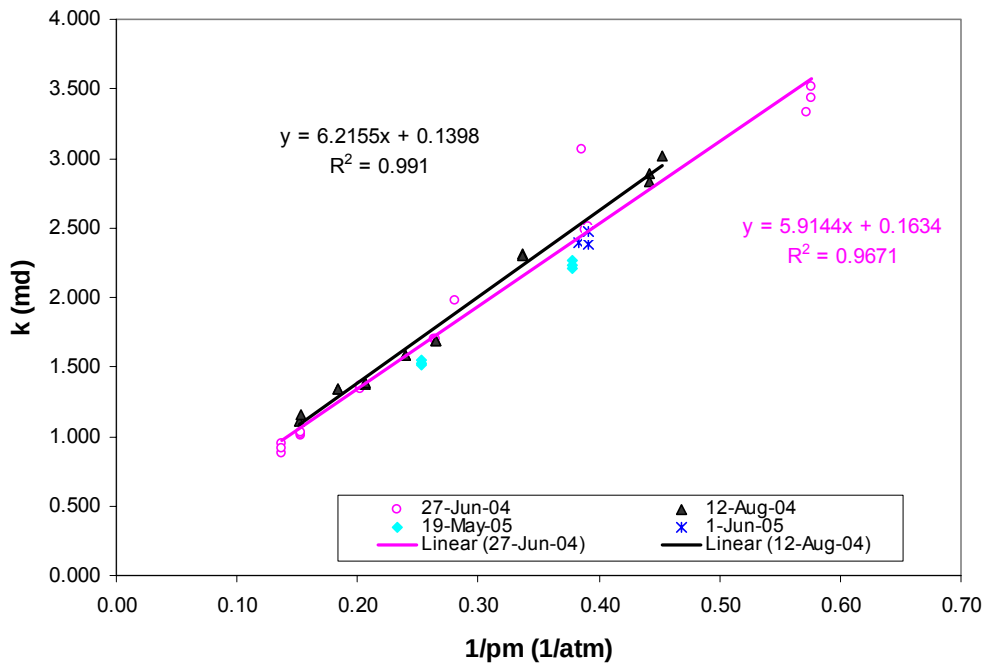

Figure 5.2: Nitrogen permeability measurements.

Chapter 6

6. Conclusion

6.1. Conclusions

This experiment confirms that component compositions do change when the gas-condensate flow pressure drops below the dew point. As the pressure drops, more of the heavier component drops out into the core, while the less heavy component will be seen in the flowing phase. After the flowing pressure drops to some point, the condensate drop-out trapped in the core starts to vaporize, at this stage, more of the heavier component will be seen in the flowing phase.

The condensate drop-out will hinder the flow capability, due to relative permeability effects. The measured decrease in the nitrogen permeability indicates the existence of the condensate drop-out even beyond the expected revaporization point and shows the permanent hindrance effect of the trapped liquid on the flow.

6.2. Future Work

Due to operational limitations, this experiment did not follow the simulation design exactly; hence it is difficult to compare the experimental work to the simulation results directly. In future experiments, the following aspects need to be considered.

1) Pressure transducer problems. Although all the pressure transducers have been calibrated under relatively high pressure, when the experiment was run under a higher pressure condition, the modified diaphragm pressure transducers still showed an unsteady response, especially the low pressure range differential transducers. The modified pressure transducers take a long time to change their response, and sometimes the pressure can not return to the normal value when the system pressure is high, even though the overall pressure difference did not exceed the transducer limit. New

transducers need to be used, or a further calibration for this kind of transducer needs to be performed.

2) This experiment confirms the composition change in the core, but how this change influences the saturation and relative permeability needs to be further addressed in future experiments.

3) The current sample port design did not provide sufficient sample volume for GC analysis; hence modified sample ports should be designed and implemented in future experiments.

4) The effects of the bottom hole pressure change or the flow rate influence on the composition and saturation change need to be further investigated.

5) The exit port of the experimental apparatus need to be modified to allow for high flow rate discharge.

Nomenclature

S_c = Condensate saturation

References

Afidick, D., Kaczorowski, N.J., and Bette, S., 1994 " Production Performance of a Retrograde Gas: A Case Study of the Arun Field," paper SPE 28749 presented at the SPE Asia Pacific Oil & Gas Conference held in Melbourne, Australia.

Barnum, R.S., Brinkman, F.P., Richadson, T.W. and Spillette, A.G., 1995 "Gas Condensate Reservoir Behavior: Productivity and Recovery Reduction Due to Condensation," paper SPE 30767 presented at the SPE Annual Technical Conference and Exhibition, Dallas, TX.

Chen, H.L., Wilson, S.D. and Monger-McClure, T.G., 1999 "Determination of Relative Permeability and Recovery for North Sea Gas-Condensate Reservoirs," paper SPE Reservoir Eval. & Eng., Vol. 2, No. 4.

Du, L., Walker, J.G., Pope, G.A., Sharma, M.M. and Wang, P, 2000 " Use of Solvents to Improve the Productivity of Gas Condensate Wells," paper SPE 62935 presented at the SPE Annual Technical Conference and Exhibition, Dallas, Texas,U.S.A.

Dullien, F.A.L., 1992 "Porous Media: Fluid Transport and Pore Structure," Academic Press.

Fevang, O., 1995 "Gas Condensate Flow Behavior and Sampling", PhD thesis, Norges Tekniske Hogskole.

Fevang, O. and Whitson, C.H., 1996 "Modeling Gas-Condensate Well Deliverability," paper SPE Res. Eng., P221-230.

Haniff, M.S. and Ali, J.K., 1990 "Relative Permeability and Low Tension Fluid Flow in Gas Condensate Systems," paper SPE 20917 presented at the SPE European Conference, Hague, Netherlands.

Mott, R., Cable, A. and Spearing, M., 1999 "A New Method of Measuring Relative Permabilities for Calculating Gas-Condensate Well Deliverability," paper SPE 56484 presented at the SPE Annual Technical Conference and Exhibition, Houston, Texas,U.S.A.

Roussennac, B., 2001 "Gas Condensate Well Test Analysis," MS report Stanford University.

Appendix A

A. List of Experiment Apparatus

Items	Quantity	Range	Model	Manufacture / Distributor
Core-holder	1	40 MPa	J300-01	Shiyi Science and Technology, China
Piston cylinder	2	4 liter, 32 MPa		Hai An, China
PR (Pressure Regulator)	1	4,000 psi	BP57-1A11C2N147 GO Reg.	Go. Company
BPR (Back Pressure Regulator)	1	4,000 psi	BP66-1B11CJN15F GO Reg.	Go. Company
Cylinder regulator (Butane)	1	max inlet: 3,000 psi; delivery pressure:-30 ~200 psi	HP 702-125-510-D	Harris Specialty Gas
Cylinder regulator (Methane)	1	max inlet 3,000 psi; delivery pressure:0-2,500 psi	8700-2500-350	Harris Specialty Gas
Pressure gauge	3	3,000 psi	PGI-63S-PG3000-LAOX	Swagelok
Pressure transducer	5	320 psi	DP15-54-N-1-S-4-A	Validyne
	2	1,250 psi	DP15-60-N-1-S-4-A	Validyne
	2	2,000 psi	DP15-62-N-1-S-4-A	Validyne
Carrier demodulator	1	8-channel	CD-280-8	Validyne
	1	4-channel	CD-280-4	Validyne
Cable assemblies	9	10' long	11581-10	Validyne
Diaphragm	4	320 psi		Validyne
Valve (needle valve)	4	3,000 psi	SS-OVS2	Swagelok
Valve (ball valve) -2 way 1/8 "	35	2,500 psi	SS-41TS2	Swagelok
Valve (ball valve) -2 way 1/4 "	1	3,000 psi	SS-43TS4	Swagelok
Valve (ball valve) -3 way	6	2,500 psi	SS-41XTS2	Swagelok
Relief valve	1	10,000 psi	SS-BVM4-C3-SH	Swagelok

Items	Quantity	Range	Model	Manufacture / Distributor
Vacuum pump	1		Welch Vacuum Pump 5	Welch
Water pump	1	10,000 psi	62-6-10	HIP
HP 5880A gas chromatograph	1			HP
Packing QC chromatogram	1		12713PC	Alltech
Gas tight syringe	2	25 µl	5182-9629	Agilent
Tedlar gas sampling bag	20	0.5 liter	232-02	SKC West
Check valve	8	25 psi	SS-2C-25	Swagelok
Test pressure gauge	1	3,000 psig	65514-33B55 GCO	3D Instruments, LLC
Safe-T-Alert 40-411	2		SM-STA-40-411-120	safehomeproducts
QRRE	1	LEL sensor	028-1000-410	RAE system

B. Eclipse input data file (constant pressure drop test)

```
-- ECLIPSE INPUT FILE
-- Production PERFORMANCE OF A L= 25.4 cm, D=5.06 cm Cylindrical core
-- Gas-condensate draw-down test
-- Permeability = 2.1 mD, Porosity = 15.0%
-- Modified 07/12/02 Add smooth krw and Pc functions
-- Simulator: Eclipse 300, 2001 v
-- The purpose is to design the Gas-condensate:
-- determine the length, permeability to get a suitable liquid
saturation distribution in the core.

RUNSPEC  ============================================================

OIL
GAS

FULLIMP

WELLDIMS
10 50 3 3 5 10 5 4 3 0 /

DIMENS
50 1 1 /

NSTACK
200/

-- condensate

ISGAS
```

```
-- Units:

LAB

-- Number of components: implies compositional run
COMPS
 2 /

MISCIBLE

GRID     ============================================================

INIT

DX
  2 49*0.51837  /
DY
  50*4.48  /

DZ
  50*4.48  /

--OLDTRAN

-- Porosity and permeability

--- (Rock)
BOX
---   IX1-IX2   JY1-JY2   KZ1-KZ2
      1   50    1   1     1   1    /
PERMX
    60000 49*2.10 /
PERMY
    60000 49*2.10 /
PERMZ
    60000 49*2.10 /
PORO
    100.0 49*0.15 /

ENDBOX

---   TOP Specification
--BOX
---   IX1-IX2   JY1-JY2  KZ1-KZ1
--    1  1     1   1    1  1 /
TOPS
     50*1 /

ENDBOX

RPTGRID
 0 0 0 0 1 1 0 0 0 1 0 0 1  /

PROPS    ============================================================

-- Properties section: PVT data from INCLUDE file

EOS
PR  /
```

```
-- Names of Components
CNAMES
C1
C4
/

-- Miscibility exponent
MISCEXP
0.000000001 /

-- Component Critical Temperatures  (K)
TCRIT
190.5611111
419.5
/

-- Component Critical Pressures   (atm)
PCRIT
45.44
36.98
/
-- Component Critical Volumes  (m3/kg-mole)
VCRIT
0.098
0.258
/

-- Component acentric factor
ACF
0.013
0.1956
/


-- Components Parachors  (dyn/cm)
--        (for IFT - Fanchi 1990)
PARACHOR
77
187.2
/

-- Peneleux Correction (Shift parameters DM-less)
SSHIFT
0.
0.
/

-- Component Molecular Weight  g/mol
MW
16.04
58.12
/

-- Binary interaction parameters
BIC
0.0
/

STCOND
15.0 1.0 /
```

```
-- Reservoir temperature: Deg C / K
RTEMP
--20  / 293.15K
20  / 293.15K

-- Rock and fluid properties

ROCK
125.0  0.00000000001  /

--Gas saturation functions
INCLUDE
KrgoGC4.dat

/

SOLUTION ==============================================================

PRESSURE

--  Pressure (atm)
50*125.0      /

SGAS
1.0 49*0.0 /

XMF
50*0.85 50*0.15  /

YMF
50*0.85 50*0.15 /

--  Calculate initial oil and gas in place at surface conditions

FIELDSEP
1 15.0 1.0 /
/

OUTSOL
 PRES SOIL XMF YMF ZMF VMF DENO DENG VOIL VGAS BOIL BGAS KRG KRO /

SUMMARY  ==============================================================

RUNSUM
--Field Gas Production Rate
FGPR
-- Field Gas Production Total
FGPT
--Well Oil Production Rate
FOPR
-- Well and Field Gas Oil Ratio
FGOR
-- Field Gas Injection Total
FGIT
-- Field Pressure
FPR


SCHEDULE ==============================================================
```

```
--SEPCOND
--SEPP  G2  1  15.0  1.0 /
/


WELLSPEC
INJ1  G1  1 1 3* /
PROD1 G2  50 1 3*   /
/

WELLCOMP
INJ1     1  1  1  1 1* 0.1 5* /
PROD1    50  1  1  1  1* 0.1 5*  /
/

-- Specify compositions of injection gas stream
WELLSTRE
LEANGAS   0.85 0.15
/
/

WCONINJE
--INJ1 GAS AUTO BHP 125. /
INJ1 GAS AUTO BHP 2* 125 /
/

WINJGAS
INJ1 STREAM LEANGAS/
/

WCONPROD
PROD1 OPEN BHP 5* 75./
--PROD1 OPEN BHP 2* 75./
/

RPTPRINT
1 1 1 2 1   1 1 1 0 0 /

RPTSCHED
PRESSURE  SOIL XMF YMF ZMF VMF DENO DENG VOIL VGAS BOIL BGAS KRG KRO /

OUTSOL
PRESSURE  SOIL XMF YMF ZMF VMF DENO DENG VOIL VGAS BOIL BGAS KRG KRO /

--TSCRIT
--0.00001 0.0000001 10
--/

TUNING
  .000277 0.05  0.0000277 /
  /
   /


TSTEP
5*0.005 5*0.01 5*0.05 5*0.1 20*0.5 10*1.0 /

END
```

C. Compressibility factor for methane

pressure (psia)	Z factor	moles	pressure (psia)	Z factor	moles
10	0.99839	0.11107	225	0.96456	2.58666
15	0.99758	0.16674	230	0.96379	2.64625
20	0.99678	0.22249	235	0.96302	2.70592
25	0.99598	0.27834	240	0.96226	2.76569
30	0.99517	0.33428	245	0.96150	2.82555
35	0.99437	0.39030	250	0.96073	2.88551
40	0.99357	0.44642	255	0.95997	2.94555
45	0.99277	0.50263	260	0.95921	3.00569
50	0.99197	0.55893	265	0.95845	3.06592
55	0.99118	0.61531	270	0.95769	3.12624
60	0.99038	0.67179	275	0.95694	3.18666
65	0.98958	0.72836	280	0.95618	3.24716
70	0.98879	0.78502	285	0.95542	3.30776
75	0.98799	0.84177	290	0.95467	3.36845
80	0.98720	0.89861	295	0.95392	3.42924
85	0.98640	0.95554	300	0.95316	3.49011
90	0.98561	1.01256	305	0.95241	3.55108
95	0.98482	1.06968	310	0.95166	3.61214
100	0.98403	1.12688	315	0.95091	3.67329
105	0.98324	1.18417	320	0.95016	3.73454
110	0.98245	1.24156	325	0.94942	3.79587
115	0.98166	1.29903	330	0.94867	3.85730
120	0.98088	1.35660	335	0.94793	3.91882
125	0.98009	1.41426	340	0.94718	3.98044
130	0.97930	1.47201	345	0.94644	4.04214
135	0.97852	1.52985	350	0.94570	4.10394
140	0.97774	1.58778	355	0.94496	4.16583
145	0.97695	1.64581	360	0.94422	4.22781
150	0.97617	1.70392	365	0.94348	4.28988
155	0.97539	1.76213	370	0.94274	4.35205
160	0.97461	1.82043	375	0.94201	4.41431
165	0.97383	1.87882	380	0.94127	4.47666
170	0.97305	1.93730	385	0.94054	4.53910
175	0.97228	1.99588	390	0.93981	4.60163
180	0.97150	2.05454	395	0.93907	4.66426
185	0.97073	2.11330	400	0.93834	4.72698
190	0.96995	2.17215	405	0.93761	4.78979
195	0.96918	2.23109	410	0.93689	4.85269
200	0.96840	2.29012	415	0.93616	4.91568
205	0.96763	2.34924	420	0.93543	4.97876
210	0.96686	2.40846	425	0.93471	5.04194
215	0.96609	2.46777	430	0.93399	5.10521
220	0.96532	2.52717	435	0.93326	5.16857

pressure (psia)	Z factor	moles	pressure (psia)	Z factor	moles
440	0.93254	5.23202	1550	0.81222	21.16147
445	0.93182	5.29556	1555	0.81189	21.23821
450	0.93110	5.35919	1560	0.81157	21.31495
455	0.93039	5.42292	1565	0.81125	21.39170
460	0.92967	5.48673	1570	0.81093	21.46845
465	0.92896	5.55064	1575	0.81062	21.54520
470	0.92824	5.61464	1580	0.81030	21.62195
475	0.92753	5.67872	1585	0.80999	21.69870
480	0.92682	5.74290	1590	0.80968	21.77546
485	0.92611	5.80717	1595	0.80938	21.85221
490	0.92540	5.87153	1600	0.80907	21.92897
495	0.92469	5.93598	1605	0.80877	22.00572
500	0.92399	6.00053	1610	0.80847	22.08247
1400	0.82295	18.86435	1615	0.80817	22.15921
1405	0.82256	18.94067	1620	0.80788	22.23596
1410	0.82217	19.01702	1625	0.80758	22.31270
1415	0.82179	19.09339	1630	0.80729	22.38943
1420	0.82140	19.16978	1635	0.80700	22.46616
1425	0.82102	19.24619	1640	0.80671	22.54289
1430	0.82064	19.32262	1645	0.80643	22.61960
1435	0.82027	19.39907	1650	0.80615	22.69632
1440	0.81989	19.47554	1655	0.80587	22.77302
1445	0.81952	19.55203	1660	0.80559	22.84971
1450	0.81915	19.62854	1665	0.80531	22.92640
1455	0.81879	19.70506	1670	0.80504	23.00308
1460	0.81842	19.78160	1675	0.80477	23.07974
1465	0.81806	19.85816	1680	0.80450	23.15640
1470	0.81770	19.93473	1685	0.80423	23.23304
1475	0.81734	20.01132	1690	0.80396	23.30968
1480	0.81698	20.08792	1695	0.80370	23.38630
1485	0.81663	20.16453	1700	0.80344	23.46290
1490	0.81627	20.24116	1705	0.80318	23.53950
1495	0.81592	20.31780	1710	0.80292	23.61608
1500	0.81558	20.39445	1715	0.80267	23.69264
1505	0.81523	20.47112	1720	0.80242	23.76919
1510	0.81489	20.54779	1725	0.80217	23.84572
1515	0.81454	20.62447	1730	0.80192	23.92224
1520	0.81421	20.70116	1735	0.80167	23.99874
1525	0.81387	20.77786	1740	0.80143	24.07522
1530	0.81353	20.85457	1745	0.80119	24.15168
1535	0.81320	20.93129	1750	0.80095	24.22812
1540	0.81287	21.00801	1755	0.80071	24.30455
1545	0.81254	21.08474	1760	0.80047	24.38095

pressure (psia)	Z factor	moles	pressure (psia)	Z factor	moles
1765	0.80024	24.45733	1885	0.79529	26.28278
1770	0.80001	24.53369	1890	0.79511	26.35846
1775	0.79978	24.61003	1895	0.79493	26.43410
1780	0.79956	24.68635	1900	0.79476	26.50971
1785	0.79933	24.76264	1905	0.79458	26.58528
1790	0.79911	24.83891	1910	0.79441	26.66082
1795	0.79889	24.91516	1915	0.79424	26.73631
1800	0.79867	24.99138	1920	0.79407	26.81177
1805	0.79845	25.06757	1925	0.79391	26.88719
1810	0.79824	25.14374	1930	0.79375	26.96257
1815	0.79803	25.21988	1935	0.79358	27.03791
1820	0.79782	25.29600	1940	0.79343	27.11322
1825	0.79761	25.37209	1945	0.79327	27.18848
1830	0.79741	25.44815	1950	0.79311	27.26370
1835	0.79720	25.52418	1955	0.79296	27.33888
1840	0.79700	25.60018	1960	0.79281	27.41402
1845	0.79680	25.67615	1965	0.79266	27.48911
1850	0.79661	25.75209	1970	0.79251	27.56416
1855	0.79641	25.82800	1975	0.79237	27.63917
1860	0.79622	25.90388	1980	0.79223	27.71414
1865	0.79603	25.97973	1985	0.79209	27.78906
1870	0.79584	26.05554	1990	0.79195	27.86394
1875	0.79566	26.13132	1995	0.79181	27.93877
1880	0.79547	26.20707	2000	0.79168	28.01355